Human tumor-associated macrophages and neutrophils regulate anti-tumor antibody efficacy through lethal and sublethal trogocytosis

Sunil Singhal[1], Abhishek S. Rao[1], Jason Stadanlick[1], Kyle Bruns[1], Neil T. Sullivan[1], Andres Bermudez[1], Adam Honig-Frand[1], Ryan Krouse[1], Sachinthani Arambepola[1], Emily Guo[1], Edmund K. Moon[2], George Georgiou[3], Tomas Valerius[4], Steven M. Albelda[2], and Evgeniy B. Eruslanov[1*].

[1]Department of Surgery, Perelman School of Medicine, University of Pennsylvania, Philadelphia, PA, USA.

[2]Department of Medicine, Perelman School of Medicine, University of Pennsylvania, Philadelphia, PA, USA.

[3]Department of Chemical Engineering, University of Texas at Austin, Austin, TX, USA

[4]Department of Medicine II, Christian Albrechts University and University Hospital Schleswig-Holstein, Kiel, Germany.

Running title: Dual role of trogocytosis mediated by FcR^+ myeloid cells

[*]Corresponding Author: Evgeniy Eruslanov,

mailing address: Stemmler Hall, 3450 Hamilton Walk, Office 408A, Department of Surgery, Perelman School of Medicine, University of Pennsylvania, Philadelphia, PA, 19104, USA

evgeniy.eruslanov@pennmedicine.upenn.edu

The authors have declared that no conflict of interest exists

Abstract

The clinical benefits of tumor-targeting antibodies (tAbs) are modest in solid human tumors. The efficacy of many tAbs is dependent on Fc Receptor (FcR)-expressing leukocytes that bind Fc fragments of tAb. Tumor-associated macrophages (TAM) and neutrophils (TAN) represent the majority of FcR^+ effectors in solid tumors. A better understanding of the mechanisms by which TAM and TAN regulate tAb response could help improve the efficacy of cancer treatments. Here, we found that myeloid effectors interacting with tAb-opsonized lung cancer cells employed antibody-dependent trogocytosis (ADT) but not antibody-dependent phagocytosis. During this process, myeloid cells "nibbled off" tumor cell fragments containing tAb/targeted antigen (tAg) complexes. ADT was only tumoricidal when the tumor cells expressed high levels of tAg and the effectors were present at high effector-to-tumor ratios. If either of these conditions were not met, which is typical for solid tumors, ADT was sublethal. Sublethal ADT, mainly mediated by $CD32^{hi}CD64^{hi}$ TAM, led to two outcomes: 1) removal of surface tAg/tAb complexes from the tumor that facilitated tumor cell escape from the tumoricidal effects of tAb and 2) acquisition of bystander tAgs by TAM with subsequent cross-presentation and stimulation of tumor-specific T cell responses. $CD89^{hi}CD32^{lo}CD64^{lo}$ peripheral blood neutrophils (PBN) and TAN stimulated tumor cell growth in the presence of the IgG1 anti-EGFR Ab cetuximab; however, IgA anti-EGFR Abs triggered the tumoricidal activity of PBN and negated the stimulatory effect of TAN. Overall, this study provides insights into the mechanisms by which myeloid effectors mediate tumor cell killing or resistance during tAb therapy.

Significance

The elucidation of the conditions and mechanisms by which human FcR^+ myeloid effectors mediate cancer cell resistance and killing during antibody treatment could help develop improved strategies for treating solid tumors.

Introduction

Antibodies that target tumor antigens (tAbs) are widely used in the treatment of human tumors; however, the clinical benefits of these tAbs are modest in most solid tumors (1). A major challenge in improving their efficacy is a lack of complete understanding of tAbs effector mechanisms because most data has been derived from murine tumor models and human studies using peripheral blood cells. Mouse studies are suboptimal because of fundamental differences between mouse and human in tumor evolution, genetic heterogeneity, immune responses, intrinsic biology of effectors, biology of Fc receptors (FcR), and their affinity to immunoglobulin G (IgG) subclasses (2-5). Studies using peripheral blood cells of cancer patients are also limited because they do not take into account the substantial effects of the tumor microenvironment (TME).

tAbs mediate tumor regression by multiple mechanisms involving the Fab and Fc fragments of the antibody (1, 6). The binding of the Fab fragment to a tumor surface receptor can interrupt oncogenic signals (1). A Fc fragment-dependent mechanism activates the complement cascade on the surface of opsonized tumor cells resulting in cell lysis (7). Opsonized tumor cells also engage FcRs expressed on myeloid and natural killer (NK) cells to induce cytotoxicity (8). This FcR^+cell-mediated effector mechanism has been defined as antibody-dependent cellular cytotoxicity (ADCC) (1, 6). Of note, efficient ADCC has only been observed in models when tumor cell lines express high levels of the tumor antigen (tAg) and the

effector cells are present at extremely high effector-to-tumor (E:T) cell ratios that are not physiologically relevant for solid tumors (9, 10). Finally, the induction of anti-tumor T cell immunity is also important. In animal models, the efficacy of tAb is severely limited in mice with compromised adaptive immunity (11). In patients, the clinical response of tAbs occurs over weeks, not over days, suggesting that both FcR^+ cells and ensuing adaptive T cell immunity are essential for the full therapeutic effects of tAb (1). Although the induction of tumor-specific T cells has been observed in cancer patients after tAb therapy (12, 13), the underlying mechanisms by which adaptive immunity is elicited in humans have not been elucidated.

Given that FcR^+ effectors play a central role in regulating the clinical efficacy of tAbs (8, 14), it is important to consider the following key pertinent variables in solid human tumors: 1) targeted tAg density, 2) availability of FcR^+ cells, 3) FcR repertoire and the level of their expression on effectors, and 4) the functional status of tumor-infiltrating FcR^+ effectors. Although the role of tumor NK cells in modulating the effector mechanisms of tAbs has been investigated (15, 16), there is little data elucidating the functional role of tumor-infiltrating myeloid cells in regulating tAb efficacy. In fact, it is still unknown whether these cells promote or prevent tumor cell resistance in the context of tAb therapy.

The effector mechanisms of tAbs in solid tumors are likely different than those in hematopoietic tumors for the several reasons. First, malignant epithelial cells in solid tumors are usually much larger than typical leukocyte-derived tumors. Second, in solid tumors, the malignant cells often form islands with tight junctions between cells (17). These physical constraints, combined with the large size of the tumor cells, could prevent myeloid effectors from mediating the antibody-dependent phagocytosis (ADP) of opsonized tumor cells that would result in their elimination. However, it is possible that under these conditions these effectors

use an alternative mechanism recently described as "FcR-mediated trogocytosis" (18-20). During this process, FcR^+ myeloid cells "nibble off" tumor cell fragments containing tAb/tAg complexes resulting in the internalization of these fragments by effectors (19, 21). To date, tAb-triggered trogocytosis (ADT) has been studied only with blood effectors and there is still no consensus on whether this process results in inhibition of tumor cell growth, especially in solid tumors (18, 21, 22). Thus, a major goal of this study was to determine whether ADT is the primary effector mechanism of human tumor-infiltrating myeloid cells and to assess its role in the regulation of tAb efficacy in solid tumors.

Currently, antibodies directed to the epidermal growth factor receptor (EGFR) are being used for patients with breast cancer, head and neck cancer, and non-small cell lung cancer (NSCLC). In NSCLC, however, the administration of anti-EGFR Abs (i.e. cetuximab) has had limited clinical response rates and marginal survival benefits (23, 24). Thus, to provide clinical relevance, we used anti-EGFR Abs and studied their FcR-mediated effector mechanisms in human lung tumors. In our study, we identified: (i) the relative contribution of tumor and blood FcR^+ myeloid populations to efficacy of tAbs, (ii) the variables in the TME that favor FcR effector-mediated tumor cell killing vs tumor escape during tAbs treatment, (iii) mechanisms by which myeloid effectors mediate tumor cell killing or promote tumor cell resistance, and (iv) the mechanism of tAg uptake from live opsonized tumor cells with subsequent stimulation of tumor-specific T cell responses.

Material and Methods

Human Subjects. A total of 208 random patients with Stage I-IV lung cancer were selected for this study. Written informed consent for collection of a portion of tumor tissue and blood for research purposes was obtained from all patients. This study was approved by the University of Pennsylvania Institutional Review Board (protocol no. 805800) and conducted in accordance with recognized ethical guidelines. All patients met the following criteria: (i) histologically confirmed pulmonary squamous cell carcinoma (SCC) or adenocarcinoma (AC), (ii) no prior chemotherapy or radiation therapy within two years, and (iii) no other active malignancy. Detailed characteristics of the patients can be found in **Supplementary Table S1 (A-F)**.

Reagents

The enzymatic cocktail for tumor digestion consisted of serum-free Leibovitz L-15 media (ThermoFisher Scientific) supplemented with 1% Penicillin-Streptomycin, Collagenase type I and IV (170 mg/L=45-60 U/mL), Collagenase type II (56 mg/L=15-20 U/mL), DNase-I (25 mg/L), and Elastase (25 mg/L) (all from Worthington Biochemical, NJ). The culture media DMEM/F-12 1:1 (HyClone, Thermo Scientific) was supplemented with 2.5 mM L-glutamine, 15 mM HEPES Buffer, 10% of Embryonic Stem (ES) Cell Screened FBS (U.S.) (HyClone, Thermo Scientific), Penicillin (100 U/ml) and Streptomycin (100 µg/mL), hereafter referred to as complete cell culture media. HLA-A*0201-restricted NY-ESO-1 (157-165, SLLMWITQV) peptide was synthesized by AnaSpec, Inc. PKH67 Green Fluorescent Cell Linker, PKH26 Red Fluorescent Cell Linker, and LPS were purchased from Sigma. Fc engineered IgA2m antibodies containing the variable regions of the EGFR antibody cetuximab were developed by Dr. Valerius

and Dr. Georgiou(25). Clinical-grade, rituximab, and cetuximab were obtained from the Pharmacy at the Hospital of the University of Pennsylvania.

Human tumor cell lines

Human epidermoid carcinoma A431 cells (#CRL-1555), human lung adenocarcinoma cell line A549 (#CCL-185), H1975 (#CRL-5908), and Burkitt's lymphoma cell line Daudi (#CCL-213) were purchased from ATCC and cultured in complete cell culture media. Authentication of cell lines was performed by ATCC using the short tandem repeat (STR) profiling.The cell lines were tested for the absence of *Mycoplasma* quarterly at the Cell Center Service of the University of Pennsylvania and used within 10 passages.

Preparation of a single-cell suspension from tumor lung tissue

Surgically-resected fresh lung tumors were processed within 20 minutes of removal from the patient. We used an optimized disaggregation method for human lung tumors that preserves the phenotype and function of the immune cells as previously described (26-29). Briefly, under sterile conditions, all areas of tissue necrosis were trimmed away. The tumor lung tissues were sliced into 1–2 mm^3 pieces with micro-dissecting scissors equipped with tungsten carbide insert blades. For enzymatic digestion, the pieces were incubated in a shaker for 45 minutes at 37°C in serum-free L-15 Leibovitz media containing enzymes (see specifics above) and 1% Penicillin-Streptomycin (Life Technologies). L-15 Leibovitz media was formulated for use in carbon dioxide-free systems. After 45 minutes, any visible tumor pieces were vigorously pipetted against the side of a 50 mL tube to enhance disaggregation and then further incubated for 30-50 minutes under the same conditions. Larger pieces of tumor tissue were permitted to settle to the bottom of the tube and the supernatant was passed through a 70 μM nylon cell strainer (BD

Falcon). The remaining pieces in the tube underwent further pipetting before being passed through the same cell strainer. After filtration, the red blood cells were lysed using 1x Red Blood Cell Lysis Buffer (Santa Cruz). The remaining cells were washed twice in RPMI supplemented with 2% FBS and re-suspended in the cell culture media. Cell viability, as determined by trypan blue exclusion or Fixable Viability Dye eFluor 450 staining, was typically >90%. If the viability of cells was less than 80%, dead cells were eliminated using a "dead cell removal kit" (130-090-101, Miltenyi Biotec Inc.).

Peripheral blood mononuclear cells isolation

Standard approaches were utilized. Peripheral blood mononuclear cells (PBMCs) were separated by 1.077 g/ml Lymphoprep (Stemcell Technologies) gradient density centrifugation of EDTA anti-coagulated whole blood collected from cancer patients and healthy donors. To account for any possible effect of tissue digestion enzymes on the function of blood FcR^+ effectors, blood was incubated with the enzymatic cocktail before gradient separation.

Isolation of cells of macrophage/monocyte lineage

We used a combination of our tumor digestion protocol and either anti-CD14 microbeads (130-050-201, Miltenyi Biotec Inc.) or FACS sorting to isolate cells of monocyte/macrophage lineage from digested tumor and peripheral blood for functional studies as previously described (28). Monocytes from PBMC of EDTA anti-coagulated peripheral blood were isolated in a similar fashion. Previously, we have demonstrated that the CD14 cells isolated from tumor lung produced TNF-α in response to LPS stimulation at levels similar to stimulated PBMC CD14 cells indicating that these cells are fully functional after isolation(28). We have shown that

isolated macrophage/monocyte lineage $CD14^+$ cells from the tumor are mostly represented by $CD206^+CD163^+HLA\text{-}DR^{hi}$ tumor-associated macrophages (TAM)(28). Nevertheless, for experiments investigating the ability of TAM to cross-present tAg, a high purity of TAM is required and thus TAM were isolated by flow cytometric cell-sorting based on the common phenotype of TAM as $CD45^+CD11b^+CD14^+HLA\text{-}DR^{hi}CD206^+$ as previously described (28). Sterile cell sorting was performed on the FACSJazz (BD Biosciences) or MoFlo Astrios (Beckman-Coulter).

Neutrophil isolation

TANs were isolated from tumor single-cell suspensions using positive selection with CD15 or CD66b antibody-conjugated magnetic microbeads (130-046-601 and 130-111-552, Miltenyi Biotec Inc.) according to the manufacturer's protocol as previously described(27, 29). PBNs were obtained from EDTA anti-coagulated peripheral blood collected from lung cancer patients during surgery or from healthy donors. The PBNs were obtained from Lymphoprep (Accu-Prep, 1.077 g/ml) density gradient centrifugation followed by erythrocyte lysis with 1x RBC Lysis Buffer. We have previously shown that PBN and TAN isolated by this approach demonstrated high cell viability with minimal enzyme-induced premature cellular activation or cleavage of myeloid cell markers(27, 29). The purity of TANs and PBNs was typically higher than 94%.

NK cell isolation

NK cells were isolated from PBMC and single cell suspension obtained from digested tumors using positive selection with CD56 antibody-conjugated magnetic microbeads (130-050-401, Miltenyi Biotec Inc.) according to the manufacturer's protocol with the following modification. Given that the CD56 molecule could also be expressed on T cells and monocyte/macrophage

lineage cells, we first depleted PBMC and tumor digest for these cells using CD3 and CD14 magnetic microbeads (130-050-101 and 130-050-201, Miltenyi Biotec Inc) followed by isolation of NK cells. The purity of NK cells isolated from blood and tumor was typically higher than 95% and 90%, respectively. We used the positive selection of NK cells because all methods using the negative selection have been developed for the isolation of NK cells from blood and are not efficient for tumor tissue.

Generation of peripheral blood monocyte-derived dendritic cells

To differentiate blood monocytes into dendritic cells (DC), $CD14^+$ cells were isolated from PBMC as described above. Purified $CD14^+$ cells were cultured in the presence of GM-CSF (25ng/ml) (300-03, PeproTech) and IL-4 (25ng/ml) (200-04, PeproTech) for 7 days in complete cell culture medium. LPS 100ng/ml (L4516, Sigma), sOX40L 50ng/ml (310-28, PeproTech), and TNF-a 20ng/ml (300-01A, PeproTech) were added at day7 for additional 24 hours, as described in detail elsewhere(30).

Flow Cytometry

Flow cytometric analysis was performed according to standard protocols. Matched isotype antibodies were used as controls. Negative gating was based on fluorescence minus one (FMO) strategy. To exclude dead cells from analysis, cells were stained with the LIVE/DEAD fixable dead cell stains (L34966, ThermoFisher Scientific).

For phenotypic and functional analysis of macrophage/monocyte lineage cells, these cells were gated on live $CD11b^+CD14^{hi}CD66b^-$cells. TAM and monocytes were gated on their definitive phenotypes $CD11b^+CD66b^-CD14^+$HLA-$DR^{hi}CD206^+$ and $CD11b^+CD66b^-CD14^+$HLA-

$DR^{int}CD206^{-}$, respectively(28). TAN and PBN were gated on their definitive phenotypes $CD11b^{+}CD66b^{+}CD15^{hi}CD14^{-}HLA\text{-}DR^{-}$. The following cell surface antibodies were utilized: anti-CD11b (clone: ICRF44, Biolegend, 301340), anti-CD4 (clone: RPA-T4, Biolegend, 300518), anti-CD8 (clone: HIT8a, Biolegend, 300914), anti-CD3 (clone:OKT3, Biolegend, 317306), anti-CD14 (clone:HCD14, Biolegend, 325632), anti-CD66b (clone: G10F5, Biolegend, 305106), anti-HLA-DR (clone: L243, Biolegend, 307618), anti-Epcam (clone: 9C4, Biolegend, 324210), anti-CD15 (clone: HI98, BD Bioscience, 551376), anti-CD45 (clone: H130, BD Bioscience, 560367), anti-CD206 (clone: 15-2, Biolegend, 321104), anti-CD163 (clone: GHI/61, Biolegend, 333608), anti-CD64 (clone:10.1, Biolegend, 305006), anti-CD32 (clone: FUN-2, Biolegend, 303208), anti-CD16 (clone:3G8, Biolegend, 302021), anti-CD89 (clone: A59, Biolegend, 354108). Antibody against Vβ13.1 TCR chain were purchased from (clone IMMU 222, Beckman Coulter, IM2292). Anti-human CD32b (FCGR2b) recombinant antibody (clone: 6G11, HPAB-0535YY) and anti-human CD32a (FCGR2a) antibody (clone IV.3, NEUT-790CQ) were purchased from Creative Biolabs, Inc. Anti-human CD32b (FCGR2b) recombinant antibody (clone: 2B6) with modified silent Fc fragment were kindly provided by Dr. Georgiou.

For intracellular staining, fixed cells stained for surface markers were permeabilized with BD Perm/Wash™ Buffer (BD Biosciences, 554723) and then stained with FITC anti-human IFN-γ (clone: 4S.B3, Biolegend, 502506) for 45 minutes at RT. All data were acquired using the BD LSRFortessa (BD Bioscience) flow cytometers or CytoFLEX S (Beckman Coulter) and analyzed using FlowJo software (TreeStar Inc.).

Flow cytometry-based killing and trogocytosis assay

To assess the tumoricidal activity of FcR^{+} effectors towards A431 and A549 tumor cell lines in

the presence or absence of anti-EGFR Abs, target cells were labeled with a cell membrane dye PKH67 Green Fluorescent Cell Linker (Sigma, PKH67GL) according to the manufacturer's protocol. PKH67-labeled tumor cells were vigorously washed with PBS and plated at 50,000 total cells /well (24-well cell culture plate). After tumor cells were allowed to adhere for at least 2 hours, the IgG1 isotype of anti-EGFR Ab (cetuximab) or IgA isotype of anti-EGFR Ab were added at concentration 1ug/ml. The nonspecific human IgG1 or IgA isotype Abs were used as a control Abs. Fifteen minutes later purified FcR^+ effectors were added to the opsonized tumor cells at specified E:T ratios in complete cell culture media. Co-cultures without anti-EGFR Abs were used as a negative control. Twelve hours later, all floating cells within the well were collected by vigorous pipetting. Adherent cells were lifted using Accutase cell detachment solution (Sigma, SCR005) by vigorous pipetting. The pooled collected cells were stained with cell-impermeant nucleic acid stain TO-PRO-3 Iodide (ThermoFisher, T3605) at 4^oC. Cell death of PKH67-labeled target cells was determined by flow cytometry as a percent of $PKH\text{-}67^+TO\text{-}PRO\text{-}3^+$ cells.

Summary graphs represent the total tumoricidal activity of effectors that includes the percent of dead/dying intact tumor cells determined as $PKH\text{-}67^+TO\text{-}PRO\text{-}3^+$ targets and tumor cells that lost their cellular integrity at the moment of measurement determined as the difference in total PKH^+ tumor cells between control and treated groups. Specifically, we first calculated the total number (#) of the remaining live targets in treated group and control group by using the following formula: # live targets = (total number added effectors + total number added targets) x (decimal remaining PKH^+ targets) x (decimal $TO\text{-}PRO3^-PKH^+$ live targets). Next, we calculated the percent of total dead cells in treated group by using the following formula: % dead targets=100% - (# live targets (treated) ÷ # live targets (control)) × 100%.

To quantify ADT, pooled cells were collected at indicated time points and stained with fluorochrome-conjugated anti-CD14 Abs, and anti-CD66b Abs to identify macrophages/monocytes and granulocytes, respectively. Anti-EGFR Ab-triggered trogocytosis was evaluated by flow cytometry as a percentage of double-positive $CD66b^{+}PKH67^{+}$ or $CD14^{+}PKH67^{+}$ TO-PRO-3^{neg} cells having acquired $PKH67^{+}$ fragments from PKH-labeled A549 or A431 tumor cells. Some experiments were performed with blocking anti-CD64 F(ab')2 (clone 10.1, Ancell, 216-520) and anti-CD32 F(ab')2 Abs (clone 7.3, Ancell, 181-520).

Incucyte live-tumor cell growth analysis

The growth of A431 and A549 tumor cell line co-cultured with indicated effectors in the presence or absence of anti-EGFR Ab was quantified over time in the IncuCyte S3 Live-Cell Analysis System (Essen BioScience, Inc.) according to the manufacturer's protocol. Briefly, A431 and A549 cell lines that were transduced to stably express GFP fluorescent protein. GFP^{hi} A431 and GFP^{hi} A549 tumor cells were sorted by flow cytometry and expanded in cell culture. For the Incucyte assay, these GFP^{hi} tumor cell lines were plated at 2500 total cells /well (96- flat bottom well plate). Tumor cells were allowed to adhere for at least 2 hours. Once tumor cells become adherent, cetuximab or IgA anti-EGFR Abs were added at a concentration of 1ug/ml. The nonspecific human IgG1 or IgA isotype Abs were used as a control Abs. Fifteen minutes later, purified FcR^{+} effectors were added to opsonized tumor cells at different E:T ratios in the complete cell culture media. Cells were co-incubated in the IncuCyte® Live-Cell imaging System for indicated time. Tumor cell growth was quantified over time by measuring Integrated fluorescence intensity (IF) of the remaining cell-associated GFP fluorescence of adherent A549 and A431 cells. Percentage of tumor cell growth inhibition and/or stimulation in the absence of

anti-EGFRAbs is calculated at 48 hrs using the formula: (FI)(A431)-FI(A431+effectors)/FI (A431)x100%, and in the presence of anti-EGFR Abs: (FI)(A431+Abs)-FI(A431+effectors+Abs)/FI(A431+Abs)x100%. The data were analyzed, and tumor cell growth curves were generated using GraphPad Prism using GraphPad Prism 9 software.

Time-lapse microscopy and live cell imaging

Daudi and A431 tumor cells were labeled with cell membrane dye PKH67 Green Fluorescent Cell Linker (Sigma) and FcR^+ effectors were labeled with cell membrane dye PKH26 Red Fluorescent Cell Linker (Sigma), according to the manufacturer's protocol. The PKH-labeled effectors and targets were plated into a poly-d-lysine-coated 8-well chamber µ-slide (Ibidi) in AIMV cell culture media with AlbuMAX Supplement (ThermoFisher). Then, the chamber slide was centrifuged at 300g for 30 seconds to facilitate cell-to-cell contact. The slides were placed in a Leica DMI4000 inverted microscope chamber at 37°C with 5% CO_2. Rituximab was added into cell co-cultures with Daudi cells and cetuximab were added into cell co-cultures with A431 tumor cells. All antibodies were used at a concentration of 1ug/ml. Time-lapse microscopy was performed using a Leica DMI4000 inverted microscope that was equipped with a Yokogawa CSU-X1 spinning disk confocal attachment. The images were taken every 5 or 15 minutes for 2 hours with Hamamatsu ImagEM 16-bit cooled EMCCD camera at 20x magnification. The videos were assembled with MetaMorph 7 software (Molecular Devices Corporation).

Generation of NY-ESO-1-specific Ly95 T cells and A549/A2-NY-ESO-1 target lung cancer cell line

The NY-ESO-1–reactive Ly95 TCR construct is an affinity-enhanced variant of the wild-type IG4 TCR identified from T cells recognizing the HLA-A2 restricted NY-ESO-1:157-165 peptide antigen. The generation of this Ly95 TCR construct and its packaging into a lentiviral vector has been described in detail earlier(31). Human T cells were isolated from PBMC of healthy volunteer donors by negative selection using RosetteSep kit (Stem Cell Technologies). Isolated T cells were stimulated with magnetic beads coated with anti-CD3/anti-CD28 at a 1:3 cell to bead ratio. T cells were transduced with lentiviral vectors at a multiplicity of infection (MOI) of approximately 5. Cells were counted and fed with complete cell culture medium every 2 days. A small portion of expanded cells was stained for flow cytometry confirmation of successful Ly95 transduction using the Vβ13.1 TCR chain antibody. Transduction of human T cells undergoing anti-CD3/CD28 mAb-coated bead activation with high titer lentivirus that encodes the Ly95 TCR recognizing NY-ESO-1 resulted in approximately 50% of TCRVb13.1^{+} CD8^{+} cells.

For target cells, we genetically modified the A549 human lung adenocarcinoma cell line to express both NY-ESO-1 protein and HLA-A*02 as described earlier(31). Briefly, the A549 cell line was transduced by a retroviral vector encoding NY-ESO-1-T2A-HLA-A*02. The transduced A549 cells were subjected to limiting dilution at 0.5 cell per well in 96-well plates. The resulting clones were tested by flow cytometry for HLA-A*02 expression using anti-HLA-A2 Abs (clone: bb7.2, Biolegend, 343306). HLA-A2 positive clones were selected and tested in co-culture with T cells expressing the NY-ESO-1 Ly95 TCR. The clones expressing HLA-A2 that could stimulate NY-ESO-1 Ly95 TCR-expressing T cells to secrete IFN-γ were pooled to generate the A549-NY-ESO-1-A2 (A549-A2-ESO) cell line. Flow sorting was performed to enrich for high HLA-A2 expressing tumor cells. The expression of intracellular NY-ESO was

analyzed by flow cytometry using NY-ESO-1 (D1Q2U) mAb (Cell Signaling) that recognizes endogenous levels of total NY-ESO-1 protein.

Antigen-presenting cell functions of TAM

To assess whether the TAM perform APC functions, freshly sorted from tumor HLA-$A2^+CD14^+CD206^+HLA\text{-}DR^{hi}$ TAM were pre-loaded with HLA-A2-restricted NY-ESO-1 (157-165, SLLMWITQV) peptide (2 μg/mL) for 1 hour. TAM were washed three times with cell culture medium and mixed with Ly95 T cells at concentration $1.5x10^5$ cells/well (96 well U-bottom plate) in ratio 1:1 in the complete cell culture media. The Ly95 T cells co-cultured with NY-ESO-1 positive (A549-A2-ESO) and negative A549 (A549) tumor cells at the same ratio were used as a positive and negative control, respectively. Eighteen hours later, NY-ESO-specific activation of the Ly95 cells was assessed by measuring intracellular IFN-γ in gated $CD8^+TCRV\beta13.1^+$ cells. Specifically, to accumulate intracellular IFN-γ, BD GolgiStop (BD Biosciences, 554724) were added into the cell cultures during the last 6 hr. The cells were collected, washed in Stain Buffer (BD Biosciences, 554656) and stained for CD8 and Ly95 TCR surface markers using anti-CD8 and anti-TCRVβ13.1 antibodies. Surface-stained cells were fixed with BD Cytofix™ Fixation Buffer (BD Biosciences, 554655) for 20 minutes. The fixed cells were permeabilized with BD Perm/Wash Buffer (BD Biosciences, 554723) and then stained with the anti-human IFN-γ. The production of IFN-γ was analyzed in gated live $CD8^+TCRV\beta13.1^+$ cells by flow cytometry.

To assess the ADT-dependent ability of TAM to uptake and cross-present bystander tAg from live opsonized targets, we mixed CD14 bead-sorted TAM from $HLA\text{-}A2^+$ donors with $EGFR^+$A549/$HLA\text{-}A2^+$NY-ESO tumor cells in the presence or absence of cetuximab (1ug/ml) at

a ratio of 1:1 in 6-well Ultra-Low Attachment plates (Corning). The same cell co-culture conditions without cetuximab were used as negative controls. Monocyte-derived DC were used as positive controls. Four hours after co-incubation, TAM were sorted from this co-culture by flow cytometry and additionally exposed to Ly95 cells at a concentration of $1.5x10^5$ cells/well (96 well U-bottom plate) in a ratio of 1:1 for 12 hours in the complete cell culture media. NY-ESO-specific activation of the Ly95 cells was assessed by measuring intracellular IFN-γ in gated $CD8^+TCRV\beta13.1^+$ cells as described above

Statistics

All data were tested for normal distribution of variables. Comparisons between two groups were assessed with a 2-tailed Student's *t*-test for paired and unpaired data if data were normally distributed. Non-parametric Wilcoxon matched-pairs test and Mann-Whitney unpaired test were used when the populations were not normally distributed. Likewise, multiple groups were analyzed by one-way analysis of variance (ANOVA) with corresponding Tukey's multiple comparison test if normally distributed, or by the Kruskal–Wallis with Dunn's multiple comparison test if not normally distributed. Non-parametric Spearman or parametric Pearson tests were used for correlation analysis. All statistical analyses were performed with GraphPad Prism 9. A p-value <0.05 was considered statistically significant.

Data availability

The data generated in this study are available within the article and its Supplementary Data files or upon request from the corresponding author.

Results

Tumor-associated neutrophils and macrophages comprise the majority of FcR^+ effectors in human lung tumors, but differentially express FcRs.

To determine subsets of FcR^+ effectors residing in lung cancers, fresh lung tumor tissue was digested using a previously described optimized approach (26). We characterized tumor-associated neutrophils (TAN) as $CD11b^+CD15^{hi}CD66b^+MPO^+Arg1^+IL\text{-}5Ra^-$cells (27, 29) and tumor-associated macrophage/monocyte lineage cells as $CD11b^+CD14^+HLA\text{-}DR^+CD66b^-$ cells that were mostly represented by $CD206^+CD163^+HLA\text{-}DR^{hi}$ tumor-associated macrophages (TAM) (28). We phenotypically defined tumor-infiltrating NK cells as $CD45^+CD56^+CD94^+CD3^-CD14^-CD19^-$cells (**Supplementary Fig. 1A)** and dendritic cells (DC) as $IRF8^{hi}HLA\text{-}DR^{hi}CD11c^+CD141^+CD14^-$ cells (**Supplementary Fig. 1B**). We found that TAN and TAM comprised the majority of all FcR^+ effectors in lung tumors **(Fig. 1A)**. The total frequencies of TAN and TAM in lung tumor digests varied from 1% to 25% of all live cells (10.1±6.7%, n=73, and 8.5±5.9%, n=89, respectively). The accumulation of NK cells in lung tumors was significantly lower (3.2±2.4%, n=92, among all live cells) and less heterogeneous compared to TAN and TAM (**Fig. 1A**). DC were minimally present (0.9 ±0.9%, n=21) (**Fig. 1A**) and thus not analyzed further. We found no significant differences in the accumulation of FcR^+ effectors in tumors of patients with early versus advanced staged disease (**Supplementary Fig. 1C**). Detailed characteristics of patients involved in flow cytometric phenotyping are shown in **Supplementary Table 1A.**

We next evaluated the types and expression of FcRs, including CD64 ($Fc_\gamma RI$), CD32 ($Fc_\gamma RII$), CD16 ($Fc_\gamma RIII$), and CD89 ($Fc\alpha RI$) on TAN and TAM in 20 patients with NSCLC. In tumors, there was a substantial upregulation of CD89 on TAN and CD32 and CD64 on TAM

compared to their counterparts in blood **(Fig. 1B-D).** TAM were also able to express CD89 but at a lower level than TAN **(Fig. 1C and D).** TAN did not express CD32 and CD64 **(Fig. 1B and D)** and dramatically downregulated CD16 that is highly expressed on peripheral blood neutrophils (PBN) **(Fig. 1C and D).**

Next, we analyzed the expression of activating CD32a and inhibitory CD32b receptors on the surface of TAM and blood monocytes using anti-CD32a ab (clone IV.3) and anti-CD32b ab (clone 6G11) that have been demonstrated to bind these FcRs with high specificity (32-34). We found that blood monocytes express CD32a at a moderate level and CD32b at a low level, whereas TAM significantly upregulated CD32b and CD32a on their surface **(Fig. 1E)**. Thus, $CD32^{hi}CD32b^{hi}$TAM co-express inhibitory and activating CD32 receptors at significantly higher levels than $CD32^{+}CD32b^{lo}$ monocytes in blood **(Fig. 1E)**.

Based on this phenotype, $CD16^{-}CD32^{hi}CD64^{hi}CD89^{+}$ TAM have the most potential to respond to tumor cells opsonized with an IgG Ab isotype. $CD16^{lo}CD32^{-/lo}CD64^{-/lo}CD89^{hi}$ TAN are unlikely to mediate isotype IgG $Fc_{\gamma}R$-mediated effector functions but could have effector functions if their CD89 was engaged by tAb of isotype IgA.

Cetuximab-triggered tumoricidal activity of tumor-infiltrating FcR^{+} effectors is impaired

Our current knowledge about the role of myeloid effectors in regulating the tAb-driven tumor cell cytotoxicity in humans is largely based on studies using peripheral blood. Thus, in this study, we evaluated the tumoricidal ability of myeloid cells in tumor in comparison with their counterparts in blood of lung cancer patients.

First, we performed a flow cytometry-based cytotoxic assay under commonly used “optimal conditions” in which a tumor cell line with a high level of the targeted tAg

(EGFR^{hi}A431 cells) are mixed with effector cells at a high 50:1 (E:T) ratio in the presence of the anti-EGFR Ab cetuximab. Given that NK cells are the principal effector cells in the blood that efficiently kill cetuximab-opsonized tumor cells (35), we used these cells as positive controls. Under these optimized conditions, blood NK cells killed an average of 75% of opsonized A431 tumor cells (**Fig. 1F** and **G**). We performed analysis of 27 NSCLC patients and found that blood monocytes were also able to kill opsonized tumor cells, although at a much lower efficiency (~30%) compared to NK cells (**Fig. 1F** and **G**). In contrast, peripheral blood neutrophils (PBN) were not capable of mediating cetuximab-triggered A431 tumor cell cytotoxicity. In tumors, TAN remained unable to kill opsonized A431 cells and TAM failed to significantly kill opsonized targets (**Fig. 1F** and **G**). Tumor NK cells still significantly killed cetuximab-opsonized A431 cells but their tumoricidal ability was dramatically decreased compared to the blood NK cells (**Fig. 1F** and **G**). There was no tumoricidal activity detected with any of the effectors in the presence of IgG1 isotype control Abs (**Supplementary Fig. 1D).** Detailed characteristics of patients involved in the evaluation of killing ability of effectors in flow cytometry-based killing assay are shown in **Supplementary Table 1B.**

Next, we investigated the effect of FcR^{+} effectors on GFP^{+} A431 tumor cell growth in the presence of cetuximab over time using the IncuCyte® Live Cell Analysis System. This analysis showed that blood NK cells efficiently eradicated tumor cells, while monocytes were able to inhibit tumor cell growth but to a lesser degree **(Fig. 1H and I)**. TAM and NK cells from tumors (n=28) had substantially decreased ability to inhibit tumor cell growth in the presence of cetuximab than their blood counterparts **(Fig. 1H and I).** Interestingly, despite the inability of TAM to directly kill the opsonized A431 tumor cells in the flow cytometry-based assay **(Fig. 1G),** TAMs from many patients could exert a tumoristatic effect during prolonged co-incubation

with opsonized A431 tumor cells at a 50:1 (E:T) ratio (**Fig. 1I).** There was no tumor cell growth inhibition observed with blood and tumor effectors in the absence of cetuximab (**Supplementary Fig. 1E**). We have previously demonstrated that tumor cells increase the survival of PBN and TAN *in vitro* up to 48 hours (27, 29) however, PBN and TAN were unable to inhibit A431 tumor cell growth in this assay. In contrast, we found that these potentially cytotoxic cells actually promoted the growth of A431 tumor cells in the presence and even in the absence of cetuximab **(Fig. 1 H and I, Supplementary Fig. 1E**). PBN isolated from lung cancer patients and heathy donors did not differ in their ability to stimulate the A431 tumor cell growth (**Supplementary Fig. 1F**). Detailed characteristics of patients involved in the evaluation of killing ability of effectors in IncuCyte killing assays are shown in **Supplementary Table 1C.**

Our correlation analyses revealed that the tumoristatic effect of TAM is significantly decreased in advanced stage of lung tumors (**Supplementary Fig. 2A**). There were no other significant correlations between the ability of FcR^+ effectors to inhibit or stimulate the tumor cell growth in the presence of cetuximab and key clinical parameters of lung cancer patients (**Supplementary Fig. 2A-D**). Also, we did not find a significant correlation between the expression of FcR on myeloid effectors and their tumoricidal activity under "favorable for killing" conditions (**Supplementary Fig. 3**).

Anti-EGFR Abs of the IgA isotype trigger the tumoricidal activity of PBN and negate TAN's stimulatory effect on the tumor cell growth.

Given, that among all FcRs, TAN highly express only CD89 (FcαRI) (**Fig. 1D**), we asked whether FcαRI ligation could trigger the tumoricidal potential of TAN against opsonized tumor cells. We thus performed an IncuCyte assay where PBN (n=49) and TAN (n=28) were co-

cultured with EGFR^{hi}A431 tumor cell line in the presence of anti-EGFR Abs of the IgA isotype. We found that PBN began to significantly inhibit the growth of A431 tumor cells (on average more than 50% killing) in the presence of IgA anti-EGFR Ab (**Fig. 1J and K, Supplementary Fig. 4A**). Noteworthy, PBN stimulated with IgA anti-EGFR Ab were able to inhibit the growth of A431 tumor cells as efficiently as blood NK cells inhibited the cetuximab-opsonized A431 targets (**Fig. 1H-K**). NK cells did not respond to A431 cell opsonized with IgA anti-EGFR Ab, because the expression of CD89 is restricted to cells of the myeloid lineage (36). In contrast to PBN, TAN did not acquire the ability to significantly inhibit A431 tumor cell growth in the presence of IgA anti-EGFR Ab (**Fig. 1J and K**). However, the stimulatory effect of TAN, as well as PBN, on A431 tumor cells was significantly reduced in the presence of IgA anti-EGFR Ab (**Fig. 1 K and Supplementary Fig. 4A**). Monocytes (n=27) and TAM (n=24) were able to inhibit the A431 cell growth in the presence of IgA anti-EGFR Ab as efficiently as in the presence of cetuximab (**Fig. 1I and K**). There was no tumoricidal activity detected with any of the effectors in the presence of IgA2 isotype control Abs **(Supplementary Fig. 4B).**

Therefore, our data show that even when appropriate FcRs are expressed, additional tumor-induced suppressive mechanisms limit the ability of TAN and TAM to kill opsonized targets.

tAb-triggered tumoricidal activity of myeloid cells depends on the level of FcR-mediated trogocytosis

During interactions with opsonized targets, myeloid effectors could employ several killing mechanisms including antibody-dependent phagocytosis (ADP) and antibody-dependent trogocytosis (ADT) (18, 37). However, whether, and to what extent myeloid effectors use these mechanisms in solid human tumors has been largely unexplored. We thus quantitatively

distinguished between ADP and ADT in cell culture while taking into account the size of the target cell. TAMs were co-cultured with either "small" $CD20^+$Daudi lymphoma cells in the presence of rituximab (anti-CD20 Abs) or with "large" $EGFR^+$A431 epithelial tumor cells in the presence of cetuximab (anti-EGFR Abs). Using the time-lapse microscopy, we determined that TAM were able to perform classical ADP and engulf rituximab-opsonized Daudi cells (**Fig. 2A, Supplementary Movie S1**), whereas the larger A431 cells could not be phagocytosed, but were subject only to ADT where TAM were able to only "gnaw off" tumor cell fragments. (**Fig. 2B, Supplementary Movie S2**).

To distinguish and quantify ADP and ADT, we labeled Daudi or A431 tumor cells with the green fluorescent dye PKH-67 and co-cultured them with TAM in the presence or absence of the appropriate tAbs (**Fig. 2C and D**). Two hours later, cells were collected and additionally stained with Abs for CD14 to identify TAM. Flow cytometry demonstrated that both TAM-mediated ADP (with Daudi cells) and ADT (with A431 cells) could be observed as double-positive $CD14^+PKH67^+$ cells **(Fig. 2C and D**). ADT could be distinguished from ADP by the following characteristics: (i) the fluorescence of the $CD14^+PKH67^+$ effectors (**Fig. 2D, red box**) is much lower than the fluorescence of PKH-67^{hi} tumor cells (**Fig. 2D, blue box**), (ii) the percent of $CD14^+PKH67^+$ effectors substantially exceeds the original number of PKH-67^{hi} tumor cells (**Fig. 2D, red box)**, and (iii) the frequency of the remaining PKH-67^{hi} tumor cells is not markedly changed (**Fig. 2D, blue box)**. Importantly, in these co-culture experiments, pre-treatment of TAM with Cytochalasin D (an actin depolymerizing agent) or adding blocking anti-CD64 and anti-CD32 F(ab')2 fragments inhibited the formation of double-positive PKH-67^+CD14^+cells (**Supplementary Fig. 4C**). These data indicate that trogocytosis reflected the

uptake of tumor cell fragments mediated by the FcR and actin cytoskeleton and was not a result of PKH dye bleeding during the effector/tumor cell contact.

Next, we evaluated the ability of blood and tumor-derived myeloid effectors to mediate ADT or ADP in parallel with their ability to kill opsonized tumor cells in a large cohort of lung cancer patients (n=43) (**Fig. 2E-L**). First, we performed these experiments under optimal killing conditions in which $EGFR^{hi}$A431 cells were mixed with effector cells at a high 50:1 (E:T) ratio in the presence of the IgG1- or IgA-isotype anti-EGFR Abs for 12 hrs. Under these conditions, none of the effectors were able to mediate ADP of A431 cells. Instead, they performed ADT, but at strikingly different levels. The different levels of ADT depended on 1) the type of myeloid cells, 2) the isotypes of tAb and involved FcR, and 3) the origin (blood vs tumor) of effectors (**Fig. 2E-L**).

Specifically, we found that PBN perform ADT in the presence of cetuximab at a much lower level than blood monocytes. The data show a lower percent and MFI of double-positive $CD66b^{+}PKH67^{+}$ PBN (**Fig. 2E, red box and F**) compared to $CD14^{+}PKH67^{+}$ monocytes (**Fig. 2G, red box and H**). However, we found that PBN can significantly increase the ADT in the presence of IgA isotype anti-EGFR Abs (**Fig. 2E, blue box and F**). Monocytes mediated ADT at a maximum level in the presence of either cetuximab or IgA anti-EGFR Abs (**Fig. 2G and H**). TAN were not able to perform ADT in the presence of cetuximab (**Fig. 2I, red box and J**), most likely due to dramatic downregulation of $Fc_{\gamma}R$ in tumor (**Fig. 1D**). However, TAN retained high expression of CD89 (**Fig. 1D**) and thus performed ADT triggered by IgA anti-EGFR Ab, although at a much lower level than PBN (**Fig. 2I, blue box and J**). The magnitude of TAM-mediated trogocytosis was decreased in the presence of cetuximab compared to blood monocytes (**Fig. 2K, red box and L**) despite the marked upregulation of $Fc_{\gamma}R$ (CD32, CD64) on TAM (**Fig.**

1D). TAM-mediated trogocytosis triggered with the IgA anti-EGFR Abs was also reduced compared to monocytes (**Fig. 2K, blue box and L**). These data indicate that the TME limits the ability of TAM and TAN to perform ADT, even if the FcRs are highly expressed. ADT was not observed with any of the effectors in the presence of IgG1 and IgA2 isotype control Abs (**Supplementary Fig. 4D**). Detailed characteristics of patients involved in the evaluation of effectors ability to perform ADT are shown in **Supplementary Table 1D.**

Next, we compared the extent of ADT related to the ability of effectors to kill opsonized $EGFR^{hi}$A431 tumor cells at a high 50:1 (E:T) ratio. The level of ADT where tumor cell death began to significantly exceed the tumor cell death in control cell cultures without effectors was termed "tumoricidal" or "lethal" ADT. Analysis revealed a strong association between the magnitude of ADT performed by PBN (n=33), monocytes (n=28), TAN (n=28) and TAM (n=26) and their ability to kill opsonized A431 tumor cells, once trogocytosis exceeded a threshold (**Fig. 3A-D**). Specifically, a significant correlation between ADT and killing of tumor cells was found in co-cultures of PBN stimulated with IgA anti-EGFR Ab (**Fig. 3A**) and with monocytes stimulated with either IgG or IgA anti-EGFR Ab (**Fig. 3B**). In these co-cultures, the killing occurred when the level of ADT exceeded 40% on average (**Fig. 2F and H, Fig. 3A and B**). PBN were not able to kill tumor cells in the presence of cetuximab because they performed ADT at sublethal levels (<40%) (**Fig. 2F and Fig. 3A**). The cetuximab-triggered sublethal ADT mediated by PBN (**Fig. 3E, Supplementary Movie S3**) and lethal ADT by monocytes (**Fig. 3F, Supplementary Movie S4**) could be also visualized by time-lapse microscopy. TAN and TAM also performed ADT triggered by IgA anti-EGFR Ab and cetuximab, although at sublethal levels (**Fig. 2I-L**) that did not result in significant tumor cell killing (**Fig. 3C and D**).

Next, we determined whether the upregulated inhibitory CD32b (Figure 1E) is involved in the reduced ability of TAM to perform ADT and killing of cetuximab-opsonized A431 tumor cells under "favorable for killing" conditions. Flow cytometry short-term and IncuCyte long-term killing assays revealed no significant differences in the ability of TAM and blood monocytes to perform ADT (**Supplementary Fig. 5A and B)** and killing in the presence or absence of two clones (2B6 and 6G11) of anti-human CD32b Abs (**Supplementary Fig. 5C and D**) that have previously been shown to have an antagonistic effect on CD32b (32, 34). These data indicate that other more dominant tumor-induced mechanisms limit the tumoricidal ability of TAM.

To more closely simulate the *in vivo* situation, we asked whether blood and tumor-derived FcR^+ effectors were able to mediate ADT and inhibit the growth of opsonized A431 cells cultured as three-dimensional tumor spheroids. Co-culturing of these FcR^+ effectors with cetuximab-opsonized A431 tumor cell spheroids **(Supplementary Fig. 6A-C)** revealed similar results obtained with A431 cells cultured as a monolayer. PBN and TAN did not mediate ADT of A431 spheroids in the presence of cetuximab **(Supplementary Fig. 6C)** and significantly stimulated the spheroid growth **(Supplementary Fig. 6A and B).** However, IgA anti-EGFR Abs triggered PBN, but not TAN, to mediate lethal ADT and inhibit the spheroid growth **(Supplementary Fig. 6D-F).**

Overall, these data demonstrate that Ab-triggered tumoricidal activity of blood monocytes PBN, TAN, and TAM towards tumor cells that express high levels of tAg depends on their ability to perform FcR-mediated ADT.

Persistent sublethal trogocytosis mediated by TAM inhibit tumor cell growth

Since TAM are not able to execute tumoricidal ADT (**Fig. 2L**) and thus directly kill tumor cells in the flow cytometry-based assay (**Fig. 1F and Fig. 3D**), we asked why TAM from some patients are able to inhibit the A431 tumor cell growth during more prolonged co-incubation (**Fig. 1I**). We hypothesized that persistent sublethal ADT caused cumulative damage to the tumor cell membrane over time, resulting in the observed late tumoristatic effect. To address this question, we co-cultured TAM with $EGFR^{hi}$A431 tumor cells in the presence of cetuximab at a 50:1 (E:T) ratio in the IncuCyte assay. In parallel, we quantified the level of ADT mediated by TAM by flow cytometry. Similar to the results described above, we discovered that TAM-mediated sublethal ADT and no direct tumor cell killing was observed in the flow cytometry-based assay (**Fig. 3D and G**). However, there was a marked tumoristatic effect in the IncuCyte long-term assay (**Fig. 3H**). Correlation analysis revealed that the inhibition of tumor growth was significantly associated with the sublethal ADT mediated by TAM (**Fig. 3I**).

Blood and tumor-derived myeloid effectors lose the ability to kill and inhibit tumor cell growth under conditions representing the solid human tumors

The data above show the potential of blood and tumor FcR^{+} effectors to kill opsonized tumor cells and inhibit their growth under "favorable for killing" conditions (tAg^{hi} and E:T ratio ^{hi}) that may exist during tAb therapy of hematological cancers. However, solid tumors likely express differing and lower levels of tAg and are heterogeneously infiltrated with TAN and TAM (**Fig. 1A**). In fact, our flow cytometric analysis of lung tumors demonstrated that the numbers of TAM or TAN do not exceed the numbers of malignant $EpCam^{+}$ cells (**Fig. 4A**), making it unlikely that they could achieve high E:T ratios. Therefore, we first sought to

determine whether the myeloid cells retain their trogocytic, tumoricidal, and/or tumoristatic activity towards opsonized EGFR^{hi}A431 tumor cells at reduced E:T ratios.

We found that regardless of E:T ratio, monocytes interacting with EGFR^{hi}A431 cells in the presence of cetuximab were still able to perform high amounts trogocytosis (>50%) (**Fig. 4B**). However, despite this high level of trogocytosis, monocytes completely lost the ability to kill cetuximab-opsonized tumor cells at a E:T ratio 2:1 (a ratio that could be realistically achieved in lung tumors). Similarly, although PBN showed high levels of trogocytosis in the presence of IgA anti-EGFR Ab, they lost their tumoricidal activity at an E:T ratio 2:1 (**Fig. 4C**). Cumulative data obtained from 14 patients showed that neither blood nor tumor myeloid cells were able to directly kill EGFR^{hi}A431tumor cells at low E:T ratio in the presence of either cetuximab or IgA anti-EGFR Abs in the FACS-based killing assay (**Fig. 4D and E).** Of note, blood, but not tumor NK cells were still able to kill even at the 2:1 ratio **(Fig. 4D).** Similarly, the IncuCyte assay demonstrated that monocytes (**Fig. 4F**), PBN (**Fig. 4G**), and TAM (**Fig. 4H**) failed to exert tumoristatic effects on EGFR^{hi}A431 tumor cells at a 2:1 E:T ratio in the presence of either cetuximab or IgA anti-EGFR Abs (**Fig. 4I and J**), although this effect was obvious at a 50:1 ratio (**Fig. 4F-H**). However, PBN (n=20) and TAN (n=20) retained the ability to significantly stimulate A431 tumor cell growth at the low E:T ratio in the presence of cetuximab, but not with IgA anti-EGFR Abs (**Fig. 4I and J**). Tumoricidal activity was not observed with any of the effectors at a E:T ratio 2:1 in the presence of IgG1 and IgA2 isotype control Abs in FACS-based and IncuCyte assays **(Supplementary Fig. 7A-C).**

Together, these data demonstrate that both a tumoricidal level of ADT and a high number of myeloid effectors are requisite for successful killing of opsonized tumors.

It has been documented that EGFR is heterogeneously expressed in human lung tumors and the therapeutic efficacy of cetuximab depends on the density of EGFR (23, 38). Indeed, our flow cytometry analysis of EGFR expression on malignant $EpCam^{+}$ cells demonstrated wide variability in the expression of EGFR in lung tumors (n=31) which is consistently higher than in a distant lung tissue (**Fig. 4K**). Thus, different levels of the targeted tAg could be another variable affecting the success of Ab-triggered tumoricidal activity of myeloid effectors in tumors. To address this issue, we utilized the human non-small cell lung cancer cell line A549 because the level of the EGFR expression was comparable to that in most lung tumors (**Fig. 4L)**. Also, A549 cells are known to be insensitive to the blockade of EGFR signaling due to the presence of a KRAS mutation (39) and are thus resistant to the Fab-mediated effect of cetuximab. Therefore, the tumoricidal mechanism of anti-EGFR Abs towards A549 cells directly depends on the FcR effectors.

Having analyzed 28 NSCLC patients, we found that PBN and monocytes co-cultured with $EGFR^{lo}$A549 cells even at a high 50:1 E:T ratio lost their ability to perform tumoricidal ADT in the presence of cetuximab or IgA anti-EGFR Abs (**Fig. 5A-C**) when compared to $EGFR^{hi}$A431 cells (**Fig. 2E-H**). This dramatic reduction in trogocytosis from the lethal to sublethal levels (or even to complete loss) resulted in the failure of monocytes and PBN to kill $EGFR^{lo}$A549 cells in the presence of cetuximab or IgA anti-EGFR Abs, respectively, even at "favorable for killing" 50:1 E:T ratio (**Fig. 5A-D**). Noteworthy, blood NK cells were still able to kill $EGFR^{lo}$A549 cells in the presence of cetuximab (**Fig. 5D**) indicating that this tumor cell line is sensitive to FcR-dependent tumoricidal mechanisms. Likewise, TAN were unable to perform ADT in co-culture with $EGFR^{lo}$A549 cells in the presence of either cetuximab or IgA anti-EGFR Abs, while TAM performed ADT at only sublethal level (**Fig. 5E-G**). As a result, no killing of

EGFR^{lo}A549 cells by TAN and TAM was detected in these co-cultures (**Fig. 5E-H**). The IncuCyte assay also confirmed the inability of blood and tumor myeloid effectors to inhibit EGFR^{lo}A549 cell growth in the presence of cetuximab or IgA anti-EGFR Abs even at a "favorable for killing" 50:1 E:T ratio (**Fig. 5I-K**). Similar to EGFR^{hi}A431 tumor cell line, PBN and TAN retained their ability to stimulate EGFR^{lo}A549 cell growth in the presence of cetuximab and IgA anti-EGFR Abs (**Fig. 5 J and K**), or even without Abs (**Fig. 5L).** There was no tumoricidal activity mediated by any of the effectors in the presence of IgG1 and IgA2 isotype control Abs in flow cytometry-based and IncuCyte-based killing assays (**Supplementary Fig. 7D-F**). Co-culturing of blood and tumor-derived FcR^{+} effectors with cetuximab-opsonized A549 tumor cell spheroids **(Supplementary Fig. 8A and B)** revealed similar results obtained with A549 cells cultured as a monolayer.

Similar results were obtained with another EGFR^{lo} tumor cell line, H-1975 (**Supplementary Fig. 8C-E)**. That is, blood and tumor myeloid effectors were not able to perform cetuximab-triggered trogocytosis at the lethal level and thus kill targets even at a "favorable for killing" 50:1 E:T ratio (**Supplementary Fig. 8D and E).**

In summary, our data demonstrate that myeloid effectors have the potential to kill opsonized tumor cells and inhibit their growth only under these three conditions: 1) the tumor cells express a high level of targeted tAg, 2) the effector cells are present at high E:T ratios, and 3) the effector cells mediate the ADT at a tumoricidal level. If these conditions are unsatisfied, the myeloid cells fail to kill sufficient numbers of opsonized tumor cells to inhibit their growth (**Fig. 5M, Supplementary Table 2)**.

Sublethal trogocytosis facilitates tumor cells to escape from tAb due to the removal of tAb/tAg complexes from the target's surface

Next, we asked what might be the functional consequences of the sublethal ADT mediated by TAM under the conditions typical for solid human tumors. We hypothesized that one effect might be that persistent sublethal trogocytosis removes tAb/tAg complexes (cetuximab/EGFR in our case) from the surface of tumor cells that might then confer resistance to subsequent attacks by NK cells due to loss of tAb/tAg complexes, thereby further reducing tAb efficacy (**Fig. 6A, scheme**).

We first determined whether the density of cetuximab/EGFR complexes on the target's surface was reduced during sublethal ADT observed in the co-culture of TAM with opsonized tumor cells. $EGFR^{hi}$A431 or $EGFR^{lo}$A549 tumor cells were pre-incubated with cetuximab and then mixed with TAM at a ratio 1:1 for 2 hours. The levels of cetuximab/EGFR complexes were then analyzed on the surface of gated $EpCam^{+}$ tumor cells and compared with opsonized targets cultured without effectors where only the natural internalization of cetuximab/EGFR could occur (40). Given that cetuximab is a humanized IgG1 anti-EGFR Ab, we used an Ab specific for the human Fc fragment of IgG that allowed us to analyze the level of cetuximab/EGFR complexes on the target. We found that the density of cetuximab/EGFR complexes on the surface of opsonized $EGFR^{hi}$A431 cells was significantly decreased after co-culture with TAM (**Fig. 6B and C**). Co-incubation of TAM with $EGFR^{lo}$A549 cells also downmodulated cetuximab/EGFR complexes (**Fig. 6C**), although to a much lesser extent due to the lower level of TAM-mediated ADT of $EGFR^{lo}$A549 cells compared to $EGFR^{hi}$A431cells (**Fig. 5F and G, Fig. 2K and L)**. Thus, TAM-mediated ADT results in the decrease of tAb/tAg complexes on the target's surface.

Next, we determined whether this TAM-mediated downmodulation of cetuximab/EGFR complexes by ADT affected the ability of NK cells to perform classical ADCC (**Fig. 6A, scheme**). We opsonized EGFR^{hi}A431 or EGFR^{lo}A549 cells with cetuximab and then pre-incubated them with freshly isolated TAM at E:T ratio 1:1 for 2 hours. Under these conditions TAM are only able to mediate the sublethal ADT but not tumor cell killing (**Fig. 4 E, Fig. 5F and H).** Two hours later, autologous blood NK cells were added to these co-cultures for additional 12 hours. We found that NK cell tumoricidal activity was significantly decreased in the presence of TAM (**Fig. 6D and E**). To further evaluate the role of TAM-mediated ADT in the inhibition of NK ADCC, we performed these experiments in the presence of blocking anti-CD64 F(ab')2 and anti-CD32 F(ab')2 Abs. The blockade of these FcγRs that are highly expressed only on TAM (**Fig. 1D**), did not trigger tumoricidal activity of TAM (**Supplementary Fig. 9A and B**), but substantially restored the ability of NK cells to kill opsonized A431 and A549 targets, indicating that FcR-mediated trogocytosis contributed to the inhibition of NK-mediated ADCC (**Fig. 6D)**. The inability of FcR blockade to fully restore the tumoricidal ability of NK cells suggests the presence of other non-FcR dependent suppressive mechanisms mediated by TAM, as described elsewhere (41). The TAM-mediated suppression of blood NK cell tumoricidal activity was more pronounced in co-culture with opsonized EGFR^{hi}A431 cells compared to EGFR^{lo}A549 cells (**Fig. 6D and E)**, most likely due to the ability of TAM to perform a higher level of ADT of EGFR^{hi}A431 (**Fig. 2K and L, Fig. 5F and G)**. The IncuCyte assay also revealed that NK cell tumoricidal activity towards cetuximab-opsonized A431 cells was more reduced in co-cultures where TAM mediated higher levels of ADT (**Fig. 6F**).

These results support the hypothesis that TAM-mediated sublethal ADT represents a mechanism of tumor cell escape from being killed by subsequent FcR^+ effectors (i.e., NK cells) during tAb treatment of solid tumors.

TAM-mediated ADT represents a new mechanism of tAg acquisition from live targets that can stimulate cognate T cells

There is compelling evidence that T cell immunity is necessary for the therapeutic effect of tAb in mice and humans (11, 42). The currently accepted mechanism (derived from murine studies) suggests that first, the opsonized tumor cells should be killed by FcR^+ effectors (8). This tumor cell killing then results in the release of tAgs that are up-taken and cross-presented by antigen-presenting cells (APC) to cognate T cells. Importantly, in all these murine studies, tumor cell lines overexpressing tAg were used. However, as we demonstrated above, human lung tumors do not usually express tAgs at high levels (**Fig. 4K**) and tumor-infiltrating effectors are not able to directly kill opsonized tumor cells (**Fig. 4E, Fig. 5H**). Nevertheless, the ability of tAb (including cetuximab) to induce tumor-specific T cells has been reported in humans (12, 13, 43). The mechanisms underlying in this process in humans are unknown and were thus explored.

We hypothesized that TAMs could acquire different tAgs during sublethal ADT where they can "nibble off" tumor cell membranes containing the cetuximab/EGFR with accompanying HLA class I/peptide membrane complexes and the surrounding tumor cell cytoplasmic fragments with intracellular "bystander" tAgs. These "antigen-loaded" TAM could then either directly present freshly captured intact tumor membrane-derived HLA-peptide complexes (cross-dressing pathway) or internalize and cross-present "bystander" tAg resulting in stimulation of cognate T cell responses (cross-presentation pathway).

To test our hypothesis, we used our published *in vitro* model allowing us to investigate human tumor antigen-specific T cell effector responses (28, 31). We transduced human T cells with a high-affinity transgenic T cell receptor (TCR) called Ly95 that recognizes an HLA-A*0201–restricted peptide sequence from the human cancer testis antigen NY-ESO-1. We also genetically modified $EGFR^{lo}$A549 human lung adenocarcinoma cells to express the NY-ESO-1 protein and HLA-A*0201 (A549/A2–NY-ESO cells) (**Fig. 7A, scheme**). When we co-cultured Ly95 cells with A549 or A549/A2–NY-ESO cells for 24 hours and measured the production of IFN-γ by the Ly95 cells (identified by an Ab against the Vβ13.1 portion of the TCR), we found that $CD8^+$TCR Vβ 13.1^+ Ly95 cells cultured with A549/A2–NY-ESO cells, but not with parental A549 cells, showed robust production of IFN-γ (**Fig. 7B**). These data demonstrated the specificity of the Ly95 cells and showed that activation is not the result of allostimulation. Importantly, the re-stimulation of purified Ly95 cells with fresh A549/A2–NY-ESO cells led to unresponsive Ly95 cells (**Fig. 7C**).

Given that the majority of effector T cells are hypofunctional in tumors (44), we first determined whether TAM presenting a relevant tumor-specific antigenic peptide were able to reinvigorate these hypofunctional T cells. We isolated TAM from HLA-$A2^+$ lung cancer patients, pulsed them with NY-ESO-$1_{157–165}$ peptide, and co-cultured them with the hypofunctional Ly95 cells purified after the first round of stimulation with A549/A2–NY-ESO cells. We found that in contrast to the second ineffective stimulation with A549/A2–NY-ESO tumor cells (**Fig. 7C and E**), HLA-$A2^+$ TAM pre-loaded with NY-$ESO_{157–165}$ peptide were able to reinvigorate these Ly95 cells to produce IFN-γ (**Fig. 7D and E**), although less efficiently when compared to the first round of stimulation with A549/A2–NY-ESO cells (**Fig. 7B and E**). Thus, TAMs expressing the relevant MHC class I/tumor peptide complexes were able to activate the tumor-specific T cells.

Next, we asked if TAM could acquire tAg from live opsonized targets. First, we explored the "cross-dressing pathway" (**Fig. 7F, scheme)**, where during sublethal cetuximab-triggered trogocytosis, TAM could remove EGFR/cetuximab complexes from the opsonized $EGFR^{lo}$A549/A2-NY-ESO targets with accompanying tumor cell membranes containing nearby cell-surface proteins, including HLA-A2/NY-ESO peptide complexes. Via this mechanism, TAM would display freshly captured tumor cell membranes containing intact HLA-A2/NY-ESO complexes on their surface and activate T cells (**Fig. 7F, scheme**). To determine whether this process was operative, we used HLA-A2 negative TAM which would not able to present processed NY-ESO to the Ly95 T cells. HLA-$A2^{neg}$ TAM were thus co-cultured with cetuximab pre-opsonized A549/A2-NY-ESO tumor cells and the presence of tumor-derived HLA-A2 complexes was analyzed on the HLA-$A2^{neg}$ TAM by flow cytometry using an anti-HLA-A2 Ab at 10, 30, 60, 120 mins, and 12 hours of cell co-culturing. We found that the highest density of tumor-derived HLA-A2 molecules could be detected on the surface of HLA-$A2^{neg}$ TAM during the initial 30 min of co-incubation with cetuximab-opsonized A549/A2-NY-ESO cells (**Fig. 7G**). However, these "trogocytosed" membrane HLA-$A2^{+}$ molecules disappeared within 2 hours of co-incubation (**Fig. 7G and H**), most likely due to internalization.

Next, we determined whether these HLA-$A2^{neg}$TAM with freshly captured tumor cell membranes were capable of directly stimulating Ly95 cells (**Fig. 7F, scheme**). We opsonized $EGFR^{lo}$A549/HLA-$A2^{+}$-NY-ESO tumor cells with cetuximab and co-incubated with HLA-$A2^{neg}$ TAM. TAM were purified from this co-culture at 30 min,120 mins and 12 hrs of co-incubation and then exposed to Ly95 T cells overnight. The same cell co-cultures without cetuximab were used as negative controls. We found that some TAM isolated from co-cultures at 30 min, but not at 120 mins, where able to stimulate Ly95 cells, although at a relatively low level

(**Supplementary Fig. 9C**). The cumulative data showed a trend but did not reach the statistical significance compared to the negative control (**Supplementary Fig. 9D**).

We next explored the cross-presentation pathway (**Fig. 7I, scheme**). We have previously demonstrated the ability of TAM isolated from some lung cancer patients to cross-present NY-ESO intact protein and activate tumor-specific effector Ly95 T cell responses (28). In this study, we determined whether cross-presentation pathway takes place following interactions of TAM with opsonized tumor cells. Specifically, during sublethal ADT, TAM could "nibble off" tumor cell membranes along with surrounding tumor cell cytoplasmic fragments containing intracellular "bystander" tAgs (NY-ESO in our case) **(Fig. 7I, scheme**). To address this hypothesis, we isolated TAM from HLA-A2$^+$ lung cancer patients and co-cultured them with the cetuximab-opsonized EGFR$^+$A549/A2-NY-ESO targets at ratio 1:1 (E:T) for 4 hours to allow the processing and cross-presentation of NY-ESO captured from A549/A2-NY-ESO tumor cells. Under these cell culture conditions, TAM perform ADT, but do not cause the tumor cell death (**Fig. 5F-H**). The same cell co-culture conditions without cetuximab were used as negative controls. Monocyte-derived DC (Mo-DC) were used as professional APC controls. Four hours after co-incubation, TAM were purified from this co-culture and exposed to Ly95 cells overnight (**Fig. 7J**). Of note, cross-dressing pathway described above is not operative in this setting because the freshly captured tumor cell-surface HLA-A2$^+$/NY-ESO complexes disappear from the TAM's surface within 2 hours of co-incubation with opsonized targets (**Fig. 7G and H**). We found that TAM isolated from some, but not all, patients were able to directly stimulate Ly95 cells, although at a lower level compared to Mo-DC (**Fig. 7J-L**). As a key control, we did not observe this Ly95 stimulatory effect of TAM incubated with non-opsonized tumor cells (**Fig. 7J-L**). Also, we were able to perform the experiments with TAM isolated from several advanced

stage (III-IV) lung patients. We found that some of TAM from patients with advanced stage disease were also able to stimulate Ly95 cells (**Fig. 7K and L**).

Next, we asked whether the ability of TAM to cross present NY-ESO depended on the level of its expression in opsonized tumor cells. To address this question, we co-cultured cetuximab-opsonized NY-ESO^{lo}A549 cells or NY-ESO^{hi}A549 cells (**Supplementary Fig. 9E**) with HLA-A2^{+} TAM at ratio 1:1. Four hours after co-incubation, TAM were purified from this co-culture and exposed to Ly95 cells overnight. We found that TAM co-cultured with cetuximab-opsonized NY-ESO^{hi}A549 cells, but not NY-ESO^{lo}A549 cells, were able to stimulate NY-ESO-specific Ly95 T cells (**Supplementary Fig. 9F-H**). These data indicate that the high expression of bystander tAg being trogocytosed with cetuximab/EGFR complexes by TAM is required for successful tAg cross-presentation and the stimulation cognate T cells. Detailed characteristics of patients involved in the evaluation of ability TAM to downregulate tAb/tAg complexes and cross-present tAg are shown in **Supplementary Table 1E.**

These data suggest that even though TAM are unable to directly kill the opsonized tumor cells, they can, under the correct conditions, acquire tAg from live opsonized targets and stimulate cognate anti-tumor T cells that have the potential to eventually kill targets.

Discussion

Therapeutic Abs targeting tumor antigens are at the forefront of cancer therapeutics. However, our knowledge about the mechanism of action of these Abs is primarily limited to mechanisms mediated by the blocking ability of the Fab fragment of Abs. Therefore, in this study, we investigated the FcR-mediated effector mechanisms of tAbs mediated by tumor-infiltrating myeloid effectors isolated from lung cancers.

Our data demonstrated that after cetuximab treatment *in vitro*, blood monocytes, but not PBN, were able to kill opsonized tumor cells. In tumors, TAM did not have tumoricidal ability, but were able to exert tumoristatic effects. However, the tumoricidal/tumoristatic activity of monocytes and TAM could only be observed under specific conditions (tAg^{hi} and E:T $ratio^{hi}$). PBN and TAN were unable to kill the cetuximab-opsonized tumor cells even under optimized conditions. The difference in cetuximab-triggered tumoricidal activity between monocytes/macrophages and PBN could be, in part, explained by differences in the expression and function of $Fc_{\gamma}Rs$. Monocytes express a high level of the intermediate to high-affinity FcγRIIa (CD32a) and FcγRI (CD64) which are the most potent FcRs for triggering tumoricidal activity (45). In contrast, PBN express lower levels of CD32 than monocytes, but abundant levels of the low-affinity FcγRIIIb receptor (CD16b). Importantly, in tumors, neutrophils dramatically downregulated all types of FcγRs and were thus unable to respond to cetuximab, while TAM upregulated CD32 and CD64 and exerted tumoristatic effects on the opsonized target. In addition, CD16b is thought to be a non-signaling $Fc_{\gamma}R$ in neutrophils, and, thus, could actually redirect IgG away from CD32 resulting in insufficient activation of PBN to deploy their formidable tumoricidal potential (46, 47). It should be noted that the low tumoricidal activity of PBN on cetuximab-opsonized tumor cells that has been reported in the literature, occurred only at an extremely high 80:1 E:T ratio (9) or after stimulation of the PBN with G(M)-CSF that dramatically upregulated the high affinity receptor CD64, thus supporting the importance of the high affinity $Fc_{\gamma}Rs$ in the activation of tumoricidal activity. In our study, resting PBN could become highly tumoricidal, but only when their highly expressed FcαRI (CD89) was engaged with an anti-EGFR Ab of isotype IgA. Our data are in concordance with other studies demonstrating that CD89 ligation with IgA isotype tAbs triggers tumoricidal activity of

neutrophils *in vitro* towards tumor cell lines expressing various tumor-associated antigens, including EGFR, Her-2/neu, and CD20 (25, 48-50). In contrast to PBN, stimulation of TAN with IgA anti-EGFR Ab did not result in significant tumor cell killing, despite the fact that CD89 was highly upregulated on TAN, indicating tumor-induced suppression. Noteworthy, the stimulatory effect of TAN on tumor cell growth was overridden by ligation with IgA anti-EGFR Abs, suggesting that TAN killing machinery was engaged but not sufficient, most likely due to effect of suppressive TME.

Importantly, with regard to cancer therapy, we found that in many lung tumors (where the number of effectors is relatively low compared to the number of tumor cells, and tumor cells do not express tAg at high levels), blood and tumor-derived myeloid effectors completely lost their ability to directly kill and inhibit tumor cell growth in the presence of either anti-EGFR Abs of isotype IgA or IgG. Our results could provide some mechanistic explanation of the large FLEX clinical trial that revealed that adding cetuximab to chemotherapy of NSCLC patients produced a clinical benefit only in individuals with high EGFR levels (23). However, EGFR expression level was only a weak predictor for cetuximab benefit in that trial. Our data suggest that the frequency of TAM in tumors should also be considered.

One of the key questions of our study was to determine mechanisms by which FcR^+ myeloid effectors killed opsonized tumor cells and how tumors cells escaped this killing. Unlike the antibody-dependent phagocytosis of opsonized "small-size" lymphocytic tumors, the interaction of myeloid effectors with opsonized "large-size" epithelial tumor cell lines led to an alternative process termed antibody-dependent trogocytosis. The preponderance of ADT over ADP is likely explained by the physical constraints of the effector being unable to engulf a large-sized epithelial tumor cell. Although the process of ADT has been only studied with peripheral

blood myeloid effectors, the functional consequences of ADT have been controversial. For instance, ADT has recently been described as a dominant tumoricidal mechanism by which PBN kill SK-BR-3 cells or A431 tumor cell lines in the presence of anti-HER2/neu or anti-EGFR Ab of isotype IgG1 or IgA (18, 51). It is important to emphasize that in these studies, pre-stimulation of PBN with G-CSF and IFN-γ was required to achieve the tumoricidal effect, and the tumoricidal effect of resting, non-primed PBN was not studied. Another study has shown that macrophage-mediated trogocytosis resulted in killing of tumor cell lines overexpressing HER-2 in the presence of the anti-HER2/neu Ab trastuzumab (52). In contrast, there have been several studies demonstrating that opsonized tumor cells are resistant to ADT performed by PBN or monocytes (22, 53, 54). In our study, we found that the effect of ADT on tumor cells could either be lethal or sublethal depending on conditions. ADT was lethal only if (i) the myeloid cells "trogocytosed" a large amount of tumor cell fragments, (ii) the myeloid cells were present at a high E:T ratio (50:1), and (iii) the tumor cells expressed a high density of the targeted tAg. If any of these conditions were not met (which is typical for solid tumors), ADT still occurred; however, its magnitude was insufficient to cause tumor cell death.

Given these observations, it was important to determine the functional outcome of the sublethal ADT that likely occurs in most lung tumors. We found that although sublethal amounts of ADT do not cause immediate tumor cell death, this process appeared to damage the tumor cell membranes resulting in a tumoristatic effect if the co-cultures had a high number of TAM and the targets expressed high levels of tAg. Under all other conditions, it appeared that the strength of trogocytic attacks were not powerful enough to cause the inhibition of tumor cell growth and, in fact, sublethal trogocytosis began to exert a pro-tumoral effect. Specifically, TAM-mediated sublethal trogocytosis substantially decreased the density of cetuximab/EGFR complexes on the

target's surface resulting in the reduced ability of NK cells to mediate classical ADCC and thereby compromising the therapeutic efficacy of cetuximab. These data are supported by clinical studies demonstrating the down-modulation of different targeted Ag in hematological cancers after tAb therapy (22, 55, 56). It has also been demonstrated that during the co-culture of rituximab-opsonized Daudi lymphoma cells and PBMC, there is an ongoing competition between monocyte-mediated trogocytosis and NK cell-mediated ADCC that eventually leads to the loss of bound rituximab and lower NK killing ability (57). These results are consistent with our data showing that a similar FcR-dependent process operates in solid tumors during the interaction of TAM with cetuximab-opsonized targets. Thus, TAM-mediated sublethal trogocytosis represents one of the resistance mechanisms to tAb treatment. However, on the other hand, it has been recently been suggested that trogocytosis-mediated down-modulation of tAg could also directly cause the death of tumor cells whose survival depends on the trogocytosis-targeted receptor for signaling (58).

In humans, tAbs do not induce massive direct tumor cell death but appear to activate tumor-specific T cell responses, that are believed to be an important anti-tumoral effector mechanism of tAb therapy (12, 13). We discovered a trogocytosis-dependent mechanism that could at least partially explain the activation of tumor-specific T cell responses in tumors where tAb do not directly kill tumors and thus the massive release of tAg to be up-taken and presented by APC is highly unlikely. During cetuximab-triggered sublethal trogocytosis, TAM acquire tumor cell fragments and membranes containing cetuximab/EGFR complexes with accompanying other "bystander" tAgs, thus potentially enabling them to present freshly captured tumor membrane-derived HLA/peptide complexes to T cells. This mechanism of acquisition and display of intact tumor-derived HLA/peptide complexes has been previously described and

termed as “MHC-I cross-dressing” (59, 60). Several studies have demonstrated that MHC-I cross-dressing may play an important role for anti-tumor $CD8^+$ T cell priming by DC (61, 62). In our experimental setting, the stimulation of tumor-specific T cells by “cross-dressed” human TAM was present, but weak, due to quick disappearance of MHC-I/peptide complexes from the TAM’s surface. Of perhaps more importance, we also observed that during sublethal trogocytosis, TAM could acquire tumor cell fragments with bystander tumor proteins and then process them to allow cross-presentation of these tAg to cognate T cells causing the stimulation of T cell responses. These stimulated tumor-specific T cells would presumably then kill targets and activate the more efficient classical mechanism of stimulated T cell responses when released tAgs from dying tumor cells are cross-presented to cognate T cells by professional APC.

There is an ongoing discussion about the ability of APC to efficiently trigger tumor-specific T cell responses, especially in human tumors. On the one hand, the poor immunogenicity of tAg and the presence of immunosuppressive macrophages and tolerogenic DC present major barriers for the induction of effective adaptive anti-tumor immunity. Conversely, there is growing evidence indicating the ability of specialized subsets of DC and macrophages in tissues and lymph nodes to cross-present tAg (63, 64). Furthermore, there is compelling evidence for the stimulatory role of tAb and FcR in the function of APC. For example, tAbs are able to trigger: 1) FcR-induced amelioration of suppressive APC in cancer patients (65), 2) FcR-mediated increases in the expression of MHC II molecules and T cell co-stimulatory molecules on APC (66), 3) FcR-mediated augmentation of the cross-priming of CD8 cells (67, 68), and 4) the immunogenicity of opsonized tumor cells (69). These studies strongly support our findings about the acquired ability of FcR-stimulated TAM to cross-present tAg and stimulate cognate T cell response during the tAb treatment.

This study has certain limitations. We investigated the role of human tumor FcR effectors in the regulation of tAb efficacy using *in vitro* and *ex vivo* models that may not faithfully reflect events in tumors of patients with cancer. However, there is no perfect *in vivo* approach to model the tumoricidal and T cell responses mediated by human FcR^+ effectors in mouse models due to various crucial differences between human and mice including Ab cross-reactivity, immunogenicity, pharmacokinetics, biology of FcR and myeloid cell effectors, and affinity to immunoglobulin G (IgG) subclasses (2-5, 70-72). To date, immunodeficient mouse models are being actively developed to overcome these limitations (73) and thus could have been suitable for evaluating direct effects of human FcR effectors on targets. However, given that human tumor-infiltrating myeloid effectors do not mediate the direct cytotoxic effect on opsonized tumor cells even *in vitro,* and that adaptive T cell immunity appears to be potent in mediating the tumoricidal effect of tAbs, these immunodeficient mice were not useful for this study. Therefore, we are unaware of any murine experimental system that can faithfully represent the biology of human FcR^+ effectors and their effects on T cell responses during tAbs therapy to yield sound and clinically relevant insights. Another limitation is that we were not able to evaluate the tAb-triggered effect of FcR effectors on primary tumor cells in our assays due to their rapid cell death in cell culture *in vitro*. Also, we could not assess the role of tumor-infiltrating DC in the regulation of tAbs efficacy because the human lung tumors accumulate a very low number of DC. However, given our data obtained with monocyte-derived DC (**Fig. 7J and L**), we speculate that tumor-infiltrating DC activated through their FcRs could also play an important role in stimulating anti-T cell responses during tAb therapy. Lastly, we studied only one type of tumor and only one tAg due to the limitation in accessing and acquisition of the freshly resected tumors from a large cohort of patients with other types of cancer.

In summary, we found that TAN and TAM comprise the majority of FcR^+ effectors in human lung tumors. However, these effectors are unable to directly kill opsonized tumor cells, but instead, could facilitate tumor cell escape from tAb therapy due to the removal of surface tAg/Ab complexes. Although there are multiple suppressive mechanisms in the TME (i.e. presence of PGE_2, TGFb, suppressive pro-tumoral TAM and TAN), an important reason for the inability of myeloid effector cells to employ their tumoricidal potential in the tumor is the absence of the requisite conditions (E:T ratio^{hi} and tAg^{hi}) that are essential for efficient killing by myeloid cells. Even fully functional blood monocytes and PBN lose their ability to kill tAbs-opsonized targets under the conditions recapitulating the TME (E:T ratio^{lo} and tAg^{lo}). To date, many different approaches have been developed to improve FcR-mediated effector mechanisms of tAbs. These approaches aimed at enhancing the Ab binding affinity to activating FcR receptors or decreasing the Ab binding to the inhibitor CD32b receptor using various types of Fc engineering to change glycosylation and amino acid residues, engineering bispecific antibodies that target two tumor Ags simultaneously, and designing Ab cross-isotype or cross-subclass exchanges (37, 74). Unfortunately, these strategies have yet not shown significant clinical improvements, most likely due to inability to overcome the presence of the "unfavorable for killing" conditions (E:T ratio^{lo} and tAg^{lo}) in human solid tumors. Thus, our data suggest that therapeutic approaches to enhance the efficacy of tAbs by stimulation of the tumoricidal activity of myeloid effectors need to be combined with strategies aimed at generating more "favorable for killing" conditions and weakening the tumor-induced suppressive mechanisms. Also, given the ability of TAM (and possibly DC) to uptake tAg from opsonized live targets, cross-present it, and subsequently stimulate the cognate T cells responses, therapeutic approaches directed to enhancing adaptive immunity could be another fruitful strategy to improve the FcR-mediated

efficacy of tAbs in human solid tumors. Indeed, our results potentially provide some new mechanistic explanations for the recently observed promising clinical activity of cetuximab combined with checkpoint inhibitors in clinical trials (75).

Author contributions

S.S., S.A. and E.E. conceived of the study. S.S., J.S., A.R., K.B., N.S., S.A., A.B., A. H.-F., R.K., E.G., and E.E., performed experiments, acquired and analyzed data. Reagents were contributed by G.G., T.V., and E.M. Manuscript preparation was performed by S.S., S.A., and E.E. Manuscript revisions were performed by all authors.

Acknowledgments

This work was supported by the NIH (RO1 CA187392-01 to E. Eruslanov) and Janssen Pharmaceuticals Inc (to E. Eruslanov). Neil T Sullivan was supported by the NIH T32 training grant (CA009140). George Georgiou acknowledges support from Clayton Foundation. We thank F. Tuluc and other members of Flow Cytometry Core Lab (Children's Hospital of Philadelphia) for technical support.

References

1. Ferris RL, Jaffee EM, and Ferrone S. Tumor antigen-targeted, monoclonal antibody-based immunotherapy: clinical response, cellular immunity, and immunoescape. *J Clin Oncol.* 2010;28(28):4390-9.
2. Mestas J, and Hughes CC. Of mice and not men: differences between mouse and human immunology. *J Immunol.* 2004;172(5):2731-8.
3. Eruslanov EB, Singhal S, and Albelda SM. Mouse versus Human Neutrophils in Cancer: A Major Knowledge Gap. *Trends Cancer.* 2017;3(2):149-60.
4. Bruhns P, and Jonsson F. Mouse and human FcR effector functions. *Immunol Rev.* 2015;268(1):25-51.
5. Loisel S, Ohresser M, Pallardy M, Dayde D, Berthou C, Cartron G, et al. Relevance, advantages and limitations of animal models used in the development of monoclonal antibodies for cancer treatment. *Crit Rev Oncol Hematol.* 2007;62(1):34-42.
6. Nimmerjahn F, Gordan S, and Lux A. FcgammaR dependent mechanisms of cytotoxic, agonistic, and neutralizing antibody activities. *Trends Immunol.* 2015;36(6):325-36.
7. Dechant M, Weisner W, Berger S, Peipp M, Beyer T, Schneider-Merck T, et al. Complement-dependent tumor cell lysis triggered by combinations of epidermal growth factor receptor antibodies. *Cancer Res.* 2008;68(13):4998-5003.
8. DiLillo DJ, and Ravetch JV. Differential Fc-Receptor Engagement Drives an Anti-tumor Vaccinal Effect. *Cell.* 2015;161(5):1035-45.
9. Trivedi S, Srivastava RM, Concha-Benavente F, Ferrone S, Garcia-Bates TM, Li J, et al. Anti-EGFR Targeted Monoclonal Antibody Isotype Influences Antitumor Cellular Immunity in Head and Neck Cancer Patients. *Clin Cancer Res.* 2016;22(21):5229-37.

10. Schneider-Merck T, Lammerts van Bueren JJ, Berger S, Rossen K, van Berkel PH, Derer S, et al. Human IgG2 antibodies against epidermal growth factor receptor effectively trigger antibody-dependent cellular cytotoxicity but, in contrast to IgG1, only by cells of myeloid lineage. *J Immunol.* 2010;184(1):512-20.

11. Park S, Jiang Z, Mortenson ED, Deng L, Radkevich-Brown O, Yang X, et al. The therapeutic effect of anti-HER2/neu antibody depends on both innate and adaptive immunity. *Cancer Cell.* 2010;18(2):160-70.

12. Hilchey SP, Hyrien O, Mosmann TR, Livingstone AM, Friedberg JW, Young F, et al. Rituximab immunotherapy results in the induction of a lymphoma idiotype-specific T-cell response in patients with follicular lymphoma: support for a "vaccinal effect" of rituximab. *Blood.* 2009;113(16):3809-12.

13. Kansy BA, Shayan G, Jie HB, Gibson SP, Lei YL, Brandau S, et al. T cell receptor richness in peripheral blood increases after cetuximab therapy and correlates with therapeutic response. *Oncoimmunology.* 2018;7(11):e1494112.

14. van Egmond M, and Bakema JE. Neutrophils as effector cells for antibody-based immunotherapy of cancer. *Semin Cancer Biol.* 2013;23(3):190-9.

15. Andre P, Denis C, Soulas C, Bourbon-Caillet C, Lopez J, Arnoux T, et al. Anti-NKG2A mAb Is a Checkpoint Inhibitor that Promotes Anti-tumor Immunity by Unleashing Both T and NK Cells. *Cell.* 2018;175(7):1731-43 e13.

16. Wang W, Erbe AK, Hank JA, Morris ZS, and Sondel PM. NK Cell-Mediated Antibody-Dependent Cellular Cytotoxicity in Cancer Immunotherapy. *Front Immunol.* 2015;6:368.

17. Onozato ML, Kovach AE, Yeap BY, Morales-Oyarvide V, Klepeis VE, Tammireddy S, et al. Tumor islands in resected early-stage lung adenocarcinomas are associated with

unique clinicopathologic and molecular characteristics and worse prognosis. *Am J Surg Pathol.* 2013;37(2):287-94.

18. Matlung HL, Babes L, Zhao XW, van Houdt M, Treffers LW, van Rees DJ, et al. Neutrophils Kill Antibody-Opsonized Cancer Cells by Trogoptosis. *Cell Rep.* 2018;23(13):3946-59 e6.

19. Pham T, Mero P, and Booth JW. Dynamics of macrophage trogocytosis of rituximab-coated B cells. *PLoS One.* 2011;6(1):e14498.

20. Beum PV, Mack DA, Pawluczkowycz AW, Lindorfer MA, and Taylor RP. Binding of rituximab, trastuzumab, cetuximab, or mAb T101 to cancer cells promotes trogocytosis mediated by THP-1 cells and monocytes. *J Immunol.* 2008;181(11):8120-32.

21. Taylor RP, and Lindorfer MA. Fcgamma-receptor-mediated trogocytosis impacts mAb-based therapies: historical precedence and recent developments. *Blood.* 2015;125(5):762-6.

22. Jones JD, Hamilton BJ, and Rigby WF. Rituximab mediates loss of CD19 on B cells in the absence of cell death. *Arthritis Rheum.* 2012;64(10):3111-8.

23. Pirker R, Pereira JR, von Pawel J, Krzakowski M, Ramlau R, Park K, et al. EGFR expression as a predictor of survival for first-line chemotherapy plus cetuximab in patients with advanced non-small-cell lung cancer: analysis of data from the phase 3 FLEX study. *Lancet Oncol.* 2012;13(1):33-42.

24. Lynch TJ, Patel T, Dreisbach L, McCleod M, Heim WJ, Hermann RC, et al. Cetuximab and first-line taxane/carboplatin chemotherapy in advanced non-small-cell lung cancer: results of the randomized multicenter phase III trial BMS099. *J Clin Oncol.* 2010;28(6):911-7.

25. Lohse S, Meyer S, Meulenbroek LA, Jansen JH, Nederend M, Kretschmer A, et al. An Anti-EGFR IgA That Displays Improved Pharmacokinetics and Myeloid Effector Cell Engagement In Vivo. *Cancer Res.* 2016;76(2):403-17.

26. Quatromoni JG, Singhal S, Bhojnagarwala P, Hancock WW, Albelda SM, and Eruslanov E. An optimized disaggregation method for human lung tumors that preserves the phenotype and function of the immune cells. *J Leukoc Biol.* 2015;97(1):201-9.

27. Eruslanov EB, Bhojnagarwala PS, Quatromoni JG, Stephen TL, Ranganathan A, Deshpande C, et al. Tumor-associated neutrophils stimulate T cell responses in early-stage human lung cancer. *J Clin Invest.* 2014;124(12):5466-80.

28. Singhal S, Stadanlick J, Annunziata MJ, Rao AS, Bhojnagarwala PS, O'Brien S, et al. Human tumor-associated monocytes/macrophages and their regulation of T cell responses in early-stage lung cancer. *Sci Transl Med.* 2019;11(479).

29. Singhal S, Bhojnagarwala PS, O'Brien S, Moon EK, Garfall AL, Rao AS, et al. Origin and Role of a Subset of Tumor-Associated Neutrophils with Antigen-Presenting Cell Features in Early-Stage Human Lung Cancer. *Cancer Cell.* 2016;30(1):120-35.

30. Lutz MB, Kukutsch N, Ogilvie AL, Rossner S, Koch F, Romani N, et al. An advanced culture method for generating large quantities of highly pure dendritic cells from mouse bone marrow. *J Immunol Methods.* 1999;223(1):77-92.

31. Moon EK, Ranganathan R, Eruslanov E, Kim S, Newick K, O'Brien S, et al. Blockade of Programmed Death 1 Augments the Ability of Human T Cells Engineered to Target NY-ESO-1 to Control Tumor Growth after Adoptive Transfer. *Clin Cancer Res.* 2016;22(2):436-47.

32. Roghanian A, Teige I, Martensson L, Cox KL, Kovacek M, Ljungars A, et al. Antagonistic human FcgammaRIIB (CD32B) antibodies have anti-tumor activity and overcome resistance to antibody therapy in vivo. *Cancer Cell.* 2015;27(4):473-88.

33. Meyer T, Robles-Carrillo L, Davila M, Brodie M, Desai H, Rivera-Amaya M, et al. CD32a antibodies induce thrombocytopenia and type II hypersensitivity reactions in FCGR2A mice. *Blood.* 2015;126(19):2230-8.

34. Veri MC, Gorlatov S, Li H, Burke S, Johnson S, Stavenhagen J, et al. Monoclonal antibodies capable of discriminating the human inhibitory Fcgamma-receptor IIB (CD32B) from the activating Fcgamma-receptor IIA (CD32A): biochemical, biological and functional characterization. *Immunology.* 2007;121(3):392-404.

35. Kurai J, Chikumi H, Hashimoto K, Yamaguchi K, Yamasaki A, Sako T, et al. Antibody-dependent cellular cytotoxicity mediated by cetuximab against lung cancer cell lines. *Clin Cancer Res.* 2007;13(5):1552-61.

36. Monteiro RC, and Van De Winkel JG. IgA Fc receptors. *Annu Rev Immunol.* 2003;21:177-204.

37. Gul N, and van Egmond M. Antibody-Dependent Phagocytosis of Tumor Cells by Macrophages: A Potent Effector Mechanism of Monoclonal Antibody Therapy of Cancer. *Cancer Res.* 2015;75(23):5008-13.

38. Seo Y, Ishii Y, Ochiai H, Fukuda K, Akimoto S, Hayashida T, et al. Cetuximab-mediated ADCC activity is correlated with the cell surface expression level of EGFR but not with the KRAS/BRAF mutational status in colorectal cancer. *Oncol Rep.* 2014;31(5):2115-22.

39. Mukohara T, Engelman JA, Hanna NH, Yeap BY, Kobayashi S, Lindeman N, et al. Differential effects of gefitinib and cetuximab on non-small-cell lung cancers bearing epidermal growth factor receptor mutations. *J Natl Cancer Inst.* 2005;97(16):1185-94.

40. Sunada H, Magun BE, Mendelsohn J, and MacLeod CL. Monoclonal antibody against epidermal growth factor receptor is internalized without stimulating receptor phosphorylation. *Proc Natl Acad Sci U S A.* 1986;83(11):3825-9.

41. Molgora M, Supino D, Mavilio D, Santoni A, Moretta L, Mantovani A, et al. The yin-yang of the interaction between myelomonocytic cells and NK cells. *Scand J Immunol.* 2018;88(3):e12705.

42. Moynihan KD, Opel CF, Szeto GL, Tzeng A, Zhu EF, Engreitz JM, et al. Eradication of large established tumors in mice by combination immunotherapy that engages innate and adaptive immune responses. *Nat Med.* 2016;22(12):1402-10.

43. Ferris RL, Lenz HJ, Trotta AM, Garcia-Foncillas J, Schulten J, Audhuy F, et al. Rationale for combination of therapeutic antibodies targeting tumor cells and immune checkpoint receptors: Harnessing innate and adaptive immunity through IgG1 isotype immune effector stimulation. *Cancer Treat Rev.* 2018;63:48-60.

44. Thommen DS, and Schumacher TN. T Cell Dysfunction in Cancer. *Cancer Cell.* 2018;33(4):547-62.

45. Valerius T, Repp R, de Wit TP, Berthold S, Platzer E, Kalden JR, et al. Involvement of the high-affinity receptor for IgG (Fc gamma RI; CD64) in enhanced tumor cell cytotoxicity of neutrophils during granulocyte colony-stimulating factor therapy. *Blood.* 1993;82(3):931-9.

46. Treffers LW, van Houdt M, Bruggeman CW, Heineke MH, Zhao XW, van der Heijden J, et al. FcgammaRIIIb Restricts Antibody-Dependent Destruction of Cancer Cells by Human Neutrophils. *Front Immunol.* 2018;9:3124.

47. Nagarajan S, Venkiteswaran K, Anderson M, Sayed U, Zhu C, and Selvaraj P. Cell-specific, activation-dependent regulation of neutrophil CD32A ligand-binding function. *Blood.* 2000;95(3):1069-77.

48. Brandsma AM, Bondza S, Evers M, Koutstaal R, Nederend M, Jansen JHM, et al. Potent Fc Receptor Signaling by IgA Leads to Superior Killing of Cancer Cells by Neutrophils Compared to IgG. *Front Immunol.* 2019;10:704.

49. Rouwendal GJ, van der Lee MM, Meyer S, Reiding KR, Schouten J, de Roo G, et al. A comparison of anti-HER2 IgA and IgG1 in vivo efficacy is facilitated by high N-glycan sialylation of the IgA. *MAbs.* 2016;8(1):74-86.

50. Pascal V, Laffleur B, Debin A, Cuvillier A, van Egmond M, Drocourt D, et al. Anti-CD20 IgA can protect mice against lymphoma development: evaluation of the direct impact of IgA and cytotoxic effector recruitment on CD20 target cells. *Haematologica.* 2012;97(11):1686-94.

51. Treffers LW, Ten Broeke T, Rosner T, Jansen JHM, van Houdt M, Kahle S, et al. IgA-Mediated Killing of Tumor Cells by Neutrophils Is Enhanced by CD47-SIRPalpha Checkpoint Inhibition. *Cancer Immunol Res.* 2020;8(1):120-30.

52. Velmurugan R, Challa DK, Ram S, Ober RJ, and Ward ES. Macrophage-Mediated Trogocytosis Leads to Death of Antibody-Opsonized Tumor Cells. *Mol Cancer Ther.* 2016;15(8):1879-89.

53. Valgardsdottir R, Cattaneo I, Klein C, Introna M, Figliuzzi M, and Golay J. Human neutrophils mediate trogocytosis rather than phagocytosis of CLL B cells opsonized with anti-CD20 antibodies. *Blood.* 2017;129(19):2636-44.

54. Beum PV, Kennedy AD, Williams ME, Lindorfer MA, and Taylor RP. The shaving reaction: rituximab/CD20 complexes are removed from mantle cell lymphoma and chronic lymphocytic leukemia cells by THP-1 monocytes. *J Immunol.* 2006;176(4):2600-9.

55. Rossi EA, Goldenberg DM, Michel R, Rossi DL, Wallace DJ, and Chang CH. Trogocytosis of multiple B-cell surface markers by CD22 targeting with epratuzumab. *Blood.* 2013;122(17):3020-9.

56. Krejcik J, Frerichs KA, Nijhof IS, van Kessel B, van Velzen JF, Bloem AC, et al. Monocytes and Granulocytes Reduce CD38 Expression Levels on Myeloma Cells in Patients Treated with Daratumumab. *Clin Cancer Res.* 2017;23(24):7498-511.

57. Beum PV, Lindorfer MA, and Taylor RP. Within peripheral blood mononuclear cells, antibody-dependent cellular cytotoxicity of rituximab-opsonized Daudi cells is promoted by NK cells and inhibited by monocytes due to shaving. *J Immunol.* 2008;181(4):2916-24.

58. Vijayaraghavan S, Lipfert L, Chevalier K, Bushey BS, Henley B, Lenhart R, et al. Amivantamab (JNJ-61186372), an Fc Enhanced EGFR/cMet Bispecific Antibody, Induces Receptor Downmodulation and Antitumor Activity by Monocyte/Macrophage Trogocytosis. *Mol Cancer Ther.* 2020;19(10):2044-56.

59. Dolan BP, Gibbs KD, Jr., and Ostrand-Rosenberg S. Dendritic cells cross-dressed with peptide MHC class I complexes prime CD8+ T cells. *J Immunol.* 2006;177(9):6018-24.

60. Wakim LM, and Bevan MJ. Cross-dressed dendritic cells drive memory CD8+ T-cell activation after viral infection. *Nature.* 2011;471(7340):629-32.

61. Duong E, Fessenden TB, Lutz E, Dinter T, Yim L, Blatt S, et al. Type I interferon activates MHC class I-dressed CD11b(+) conventional dendritic cells to promote protective anti-tumor CD8(+) T cell immunity. *Immunity.* 2022;55(2):308-23 e9.

62. MacNabb BW, Tumuluru S, Chen X, Godfrey J, Kasal DN, Yu J, et al. Dendritic cells can prime anti-tumor CD8(+) T cell responses through major histocompatibility complex cross-dressing. *Immunity.* 2022.

63. Roberts EW, Broz ML, Binnewies M, Headley MB, Nelson AE, Wolf DM, et al. Critical Role for CD103(+)/CD141(+) Dendritic Cells Bearing CCR7 for Tumor Antigen Trafficking and Priming of T Cell Immunity in Melanoma. *Cancer Cell.* 2016;30(2):324-36.

64. Asano K, Nabeyama A, Miyake Y, Qiu CH, Kurita A, Tomura M, et al. CD169-positive macrophages dominate antitumor immunity by crosspresenting dead cell-associated antigens. *Immunity.* 2011;34(1):85-95.

65. Li J, Srivastava RM, Ettyreddy A, and Ferris RL. Cetuximab ameliorates suppressive phenotypes of myeloid antigen presenting cells in head and neck cancer patients. *J Immunother Cancer.* 2015;3:54.

66. Junker F, Gordon J, and Qureshi O. Fc Gamma Receptors and Their Role in Antigen Uptake, Presentation, and T Cell Activation. *Front Immunol.* 2020;11:1393.

67. Dhodapkar KM, Krasovsky J, Williamson B, and Dhodapkar MV. Antitumor monoclonal antibodies enhance cross-presentation ofcCellular antigens and the generation of myeloma-specific killer T cells by dendritic cells. *J Exp Med.* 2002;195(1):125-33.

68. Kalergis AM, and Ravetch JV. Inducing tumor immunity through the selective engagement of activating Fcgamma receptors on dendritic cells. *J Exp Med.* 2002;195(12):1653-9.

69. Pozzi C, Cuomo A, Spadoni I, Magni E, Silvola A, Conte A, et al. The EGFR-specific antibody cetuximab combined with chemotherapy triggers immunogenic cell death. *Nat Med.* 2016;22(6):624-31.

70. Masopust D, Sivula CP, and Jameson SC. Of Mice, Dirty Mice, and Men: Using Mice To Understand Human Immunology. *J Immunol.* 2017;199(2):383-8.

71. Zschaler J, Schlorke D, and Arnhold J. Differences in innate immune response between man and mouse. *Crit Rev Immunol.* 2014;34(5):433-54.

72. Nauseef WM. Human neutrophils not equal murine neutrophils: Does it matter? *Immunol Rev.* 2022.

73. Chuprin J, Buettner H, Seedhom MO, Greiner DL, Keck JG, Ishikawa F, et al. Humanized mouse models for immuno-oncology research. *Nat Rev Clin Oncol.* 2023.

74. Dixon KJ, Wu J, and Walcheck B. Engineering Anti-Tumor Monoclonal Antibodies and Fc Receptors to Enhance ADCC by Human NK Cells. *Cancers (Basel).* 2021;13(2).

75. Sacco AG, Chen R, Worden FP, Wong DJL, Adkins D, Swiecicki P, et al. Pembrolizumab plus cetuximab in patients with recurrent or metastatic head and neck squamous cell carcinoma: an open-label, multi-arm, non-randomised, multicentre, phase 2 trial. *Lancet Oncol.* 2021;22(6):883-92.

Figure 1. Accumulation, FcR expression, and tumoricidal activity of tumor-infiltrating myeloid cells. (A) Frequencies of indicated FcR^+ effectors in lung tumors analyzed by flow cytometry in a single-cell suspension obtained from digested lung tumors. (**B-D**) Representative dotplots and cumulative flow cytometry results showing the expression of the indicated FcRs on myeloid effectors in blood and tumors. MFI-mean fluorescence intensity. **(E)** Representative dotplots and cumulative flow cytometry results showing the expression of CD32a and CD32b molecules on the surface of gated $CD14^+$HLA-$DR^{int}CD206^-$ blood monocytes and $CD14^+$HLA-$DR^{hi}CD206^+$ TAM. Cells stained with isotype control Abs were used to set the gates. Wilcoxon matched paired test. (**F and G**) Representative dotplots and cumulative flow cytometry results showing the ability of blood and tumor FcR^+ effectors to kill PKH-67^+A431 tumor cells in the presence of cetuximab (1ug/ml) at a 50:1 E:T ratio in a 12 hrs assay. Dead A431 tumor cells were defined as TO-PRO-3^+PKH67^+ cells. Summary graphs represent the total tumoricidal activity of effectors calculated as described in material and methods. (**H and I**) Representative images of GFP^+A431 tumor cells co-cultured with indicated blood effectors (patient LC441) and cetuximab for 48 hrs in the IncuCyte® Live Cell Analysis System. Scale bar, 400 μm. Representative experiment (H) and summary results (I) showing the kinetics of GFP^+A431 tumor cell growth during co-culturing with blood and tumor FcR^+ effectors at a 50:1 E:T ratio in the presence of cetuximab (1ug/ml) and **(J and K)** in the presence of IgA anti-EGFR Ab (1ug/ml) in the IncuCyte® Live Cell Analysis System. Percentage of tumor cell growth inhibition/stimulation in the presence of anti-EGFR Abs was calculated at 48 hrs using the formula: (FI)(A431+Ab)-FI(A431+effectors+Ab)/FI(A431+Ab) x100%, FI-Integrated fluorescence intensity. Number of patients included in each analysis is indicated on the graphs.

All data are represented as mean ± SEM. All comparisons used one-way ANOVA with Turkey's multiple comparisons tests. FcR^+ effectors were freshly isolated for all experiments.

Figure 2. Anti-EGFR Ab-triggered trogocytosis and tumoricidal activity mediated by blood and tumor myeloid cells (A and B) Representative images (taken from time-lapse microscopy supplementary movie S1 and movie S2 at the 30 min after recording) showing the TAM-mediated phagocytosis of rituximab-opsonized Daudi tumor cells (A) and trogocytosis of cetuximab-opsonized A431 tumor cells (B). PKH26-labeled TAM (red) were incubated with opsonized PKH67-labeled targets (green) at a 3:1 E:T ratio. Scale bar, 10 μm (**C and D**) Representative dotplots demonstrating TAM-mediated phagocytosis of Daudi tumor cells in the presence or absence of rituximab (1ug/ml) (C) and trogocytosis of A431 tumor cells in the presence or absence of cetuximab (1ug/ml) (D). TAM were co-cultured with PKH67-labeled targets at 3:1 E:T ratio for 2 hrs. (**E-L**) Representative dotplots showing the different levels of trogocytosis and killing activity mediated by indicated blood and tumor myeloid effectors co-cultured with $PKH67^+$A431 cells at a 50:1 E:T ratio in the presence or absence of cetuximab (IgG1) or IgA anti-EGFR Abs (IgA) for 12 hrs. (**F, H, J, L**) Summary results of experiments described above in (E-L). Unpaired t test. Number of patients included in each analysis is indicated on the graphs. All data represented as mean ± SEM. FcR^+ effectors were freshly isolated for all experiments.

Figure 3. The lethal and sublethal effects of ADT on A431 tumor cells mediated by blood and tumor myeloid cells in the presence of anti-EGFR Abs. (**A-D**) Correlation of the ability of indicated blood and tumor myeloid effectors to mediate ADT with their ability to kill A431 tumor cells in the presence of anti-EGFR Abs determined by flow cytometry. Pearson test. (**E and F**) Images (taken from time-lapse microscopy supplementary movie S3 and movie S4 at the indicated time points after recording) showing the different amount of cetuximab-triggered trogocytic uptake of tumor cell fragments by PKH26-labeled effectors (red) PBN (E) and monocytes (F) during their interaction with PKH67-labeled A431 targets (green). Scale bar, 10 µm. (**G**) Representative dotplots demonstrating trogocytosis and killing activity mediated by TAM co-cultured with PKH67-labeled A431 cells at a 50:1 E:T ratio in the presence of cetuximab for 12 hrs. (**H**) Representative experiment showing the kinetics of GFP^+A431 tumor cell growth with TAM at a 50:1 E:T ratio in the presence or absence of cetuximab in the IncuCyte® Live Cell Analysis System. (**I**) Summary results showing the correlation between the abilities of TAM to mediate ADT and regulate A431 tumor cell growth in the presence of cetuximab in the IncuCyte® Live Cell Analysis System. Pearson test. Number of patients included in each analysis is indicated on the graphs. FcR^+ effectors were freshly isolated for all experiments

Figure 4. The ability of blood and tumor myeloid cells to perform ADT and kill EGFR^{hi} A431 cells in the presence of anti-EGFR Abs under conditions representing solid human tumors. (A) The frequencies of CD45$^-$EpCam$^+$cells, CD14$^+$CD206$^+$HLA-DR^{hi}TAM, and CD11b$^+$CD66b$^+$CD14$^-$TAN were analyzed by flow cytometry in digested lung tumors. Paired t-test. (**B** and **C**) Representative dotplots showing the levels of trogocytosis and killing activity mediated by blood monocytes (B) and PBN (C) co-cultured with PKH67$^+$ A431 cells at the indicated E:T ratios in the presence of cetuximab and IgA anti-EGFR Abs, respectively for 12 hrs. Nonspecific human IgG1 or IgA2 isotype control Abs were used as a control. (**D** and **E**) Cumulative flow cytometry results showing the ability of indicated FcR$^+$ effectors to kill PKH67$^+$ A431 tumor cells in the presence of cetuximab (IgG) or IgA anti-EGFR (IgA) Abs at a 2:1 E:T ratio in a 12 hr FACS-based assay. One-way ANOVA with Turkey's multiple comparisons tests. Summary graphs represent the total tumoricidal activity of effectors calculated as described in material and methods. (**F-H**) Representative images of GFP$^+$A431 tumor cells co-cultured with blood monocytes (patient LC441) at different E:T ratios and cetuximab for 48 hrs in the IncuCyte® Live Cell Analysis System. Image of (A431+Ab, where Ab is a cetuximab) is intentionally the same in both Fig. 1H and Fig. 4F. Scale bar, 400 µm. Representative experiments showing the kinetics of A431 tumor cell growth when co-cultured with blood monocytes (F), PBN (G), and TAM (H) in the presence of anti-EGFR Abs at the indicated E:T ratios in the IncuCyte® Live Cell Analysis System. **(I and J**) Summary results showing the kinetics of GFP$^+$A431 tumor cell growth when co-cultured with FcR$^+$ effectors in the presence of cetuximab or IgA anti-EGFR Ab at 2:1 E:T ratio in the IncuCyte® Live Cell System. Percentage of tumor cell growth inhibition/stimulation was calculated at 48 hrs. One-way ANOVA with Turkey's multiple comparisons tests. (**K**) Representative dotplots and

cumulative flow cytometry data demonstrating the expression of EGFR on the surface of $EpCam^+$ cells in tumor and distant lung tissue. Paired t-test. MFI-mean fluorescence intensity. (**L**) Representative flow cytometry histograms showing the expression of EGFR on the surface of $EpCam^+$ cells in tumor and distant lung tissue in comparison with A431 and A549 tumor cells. Number of patients is indicated on the graphs. All data represented as mean ± SEM. FcR^+ effectors were freshly isolated for all experiments.

Figure 5. The ability of blood and tumor myeloid cells to perform ADT and kill EGFR^{lo} A549 cells in the presence of anti-EGFR Abs under conditions representing solid human tumors. (**A-H**) Representative dotplots and cumulative flow cytometry results showing the different levels of ADT and killing activity mediated by PBN (A, C, D), blood monocytes (B, C, D), TAN (E, G, H), and TAM (F, G, H) co-cultured with PKH67^{+}A549 cells at a 50:1 E:T ratio in the presence or absence of cetuximab (IgG) or IgA anti-EGFR Abs (IgA) for 12 hrs. Summary graphs represent the total tumoricidal activity of effectors calculated as described in material and methods. (**I, J**, and **K**) Representative experiment and summary results showing the kinetics of A549 tumor cell growth when co-cultured with indicated blood and tumor FcR^{+} effectors in the presence of cetuximab or IgA anti-EGFR Abs at a 50:1 E:T ratio in the IncuCyte® Live Cell Analysis System. Percentage of tumor cell growth inhibition/stimulation was calculated at 48 hrs. (**L**) Cumulative results showing the kinetics of A549 tumor cell growth co-cultured with blood and tumor FcR^{+} effectors at a 50:1 E:T ratio in the presence of human IgG1 isotype control Abs in the IncuCyte® Live Cell Analysis System. Number of patients included in each analysis is indicated on the graphs. All data represented as mean ± SEM. All comparisons used one-way ANOVA with Turkey's multiple comparisons tests. FcR^{+} effectors were freshly isolated for all experiments. (**M**) The schematic representation of requisite conditions in TME that are essential for efficient killing of opsonized tumors by FcR^{+} effectors or tumor escape from tAbs. Scheme was created with BioRender.com

Figure 6. Role of TAM-mediated ADT in facilitating tumor cell escape from tAbs. (A) Scheme proposing the role of TAM-mediated ADT in the downmodulation of cetuximab/EGFR complexes on the surface of opsonized tumor cells that could lead to resistance of targets to subsequent attacks by NK cells. Scheme was created with BioRender.com (**B**) Representative flow cytometry histograms showing the expression of cetuximab/EGFR complexes on the surface of cetuximab-opsonized A431 cells co-cultured in the presence or absence of TAM at a 1:1 E:T ratio for 2 hrs. (**C**) Cumulative results showing the expression of cetuximab/EGFR complexes on the surface of cetuximab-opsonized A431 and A549 cells co-cultured in the presence or absence TAM at a 1:1 E:T ratio for 2 hrs. Wilcoxon matched-pairs signed rank test. (**D and E**) Representative dotplots and cumulative flow cytometry data demonstrating the reduced ability of blood NK cells to kill cetuximab-opsonized A431 and A549 tumor cells in the presence of TAM. Tumor cell lines were pre-opsonized with cetuximab and mixed with TAM at a 1:1 E:T ratio, two hours later NK cells were added at a 10:1 E:T ratio for additional 12 hrs. Wilcoxon matched pairs signed rank test. Some experiments were performed with blocking anti-CD64 F(ab')2 and anti-CD32 F(ab')2 Abs (5ug/ml) and representative dotplots from one of three these experiments are shown. (**F**) The kinetics of A431 tumor cell growth when co-cultured with TAM and blood NK cells in the presence of cetuximab in the IncuCyte Live Cell Analysis System. A431 cells were pre-opsonized with cetuximab and mixed with TAM at a 3:1 E:T ratio, two hours later NK cells were added at a 10:1 E:T ratio for additional 12 hrs. The ability of TAM to mediate ADT was assessed by flow cytometry in the co-cultures of TAM and cetuximab-opsonized $PKH67^{+}$A431 cells as described earlier. Two patients (LC#643 and LC#649) are

shown. All data represented as mean ± SEM. FcR^+ effectors were freshly isolated for all experiments.

Figure 7. Role of TAM-mediated ADT in tAg uptake from live opsonized targets following stimulation of tumor-specific T cells. (A) Scheme showing the in vitro model of human tumor antigen-specific T cell responses (A549/HLA-$A2^+$NY-ESO tumor cells interacting with NY-ESO specific Ly95 T cells). (**B**) Representative dot plots demonstrating the Ly95 ($CD8^+$TCR Vβ13.1^+) cells and their NY-ESO–specific IFN-γ production after exposure to A549/HLA-$A2^+$NY-ESO tumor cells compared to control A549 cells after the first round of stimulation. (**C and D**) Schemes and representative dotplots showing the second round of stimulation of purified Ly95 cells with A549/HLA-$A2^+$NY-ESO tumor cells (C) or HLA-$A2^+$TAM pre-loaded with NY-$ESO_{157–165}$ peptide (D) and the production of IFN-γ by Ly95 cells in response to the second round of the stimulation. (**E**) Cumulative data of the experiments described in (B, C and D) demonstrating the Ly95 cell responses after the 1^{st} and 2^{nd} round of stimulation (intracellular IFN-γ production). Kruskal-Wallis multiple comparison test. (**F**) Scheme showing the ADT-dependent mechanism of Ly95 cell stimulation by HLA-$A2^{neg}$ TAM that trogocytosed and displayed on their surface the A549 tumor cell membranes containing the surface cetuximab/EGFR and bystander HLA-A2/NY-ESO complexes (pathway#1, cross-dressing). (**G and H**) Representative dotplots and summary results demonstrating the acquisition and display of HLA-A2 molecules on the surface of HLA-$A2^{neg}$ TAM during their interaction with cetuximab-opsonized A549/HLA-$A2^+$NY-ESO cells at a 1:1 E:T ratio at the indicated time points. Kruskal-Wallis multiple comparisons test. Data represented as mean ± SEM. (**I**) Scheme showing the ADT-dependent mechanism of Ly95 cell stimulation by HLA-$A2^+$ TAM that

trogocytosed A549 tumor cell fragments containing cetuximab/EGFR and bystander intact NY-ESO Ag followed by the cross-presentation to Ly95 cells (pathway#2, cross-presentation). (**J, K,** and **L**) Representative dotplots and cumulative data showing the ability of HLA-$A2^+$ TAM (from early and advanced stage lung cancers) to stimulate of Ly95 cells responses (intracellular IFN-γ) after preincubation with A549/HLA-$A2^+$NY-ESO tumor cells in the presence or absence of cetuximab for 4 hrs. Mo-DC used as a professional APC. Wilcoxon matched pairs test for groups with (+) or without (-) Ab. * $p<0,01$. Kruskal-Wallis test for groups with Mo-DC, early-stage TAM, and advanced stage TAM. FcR^+ effectors were freshly isolated for all experiments. All schemes were created with BioRender.com

Figure 1

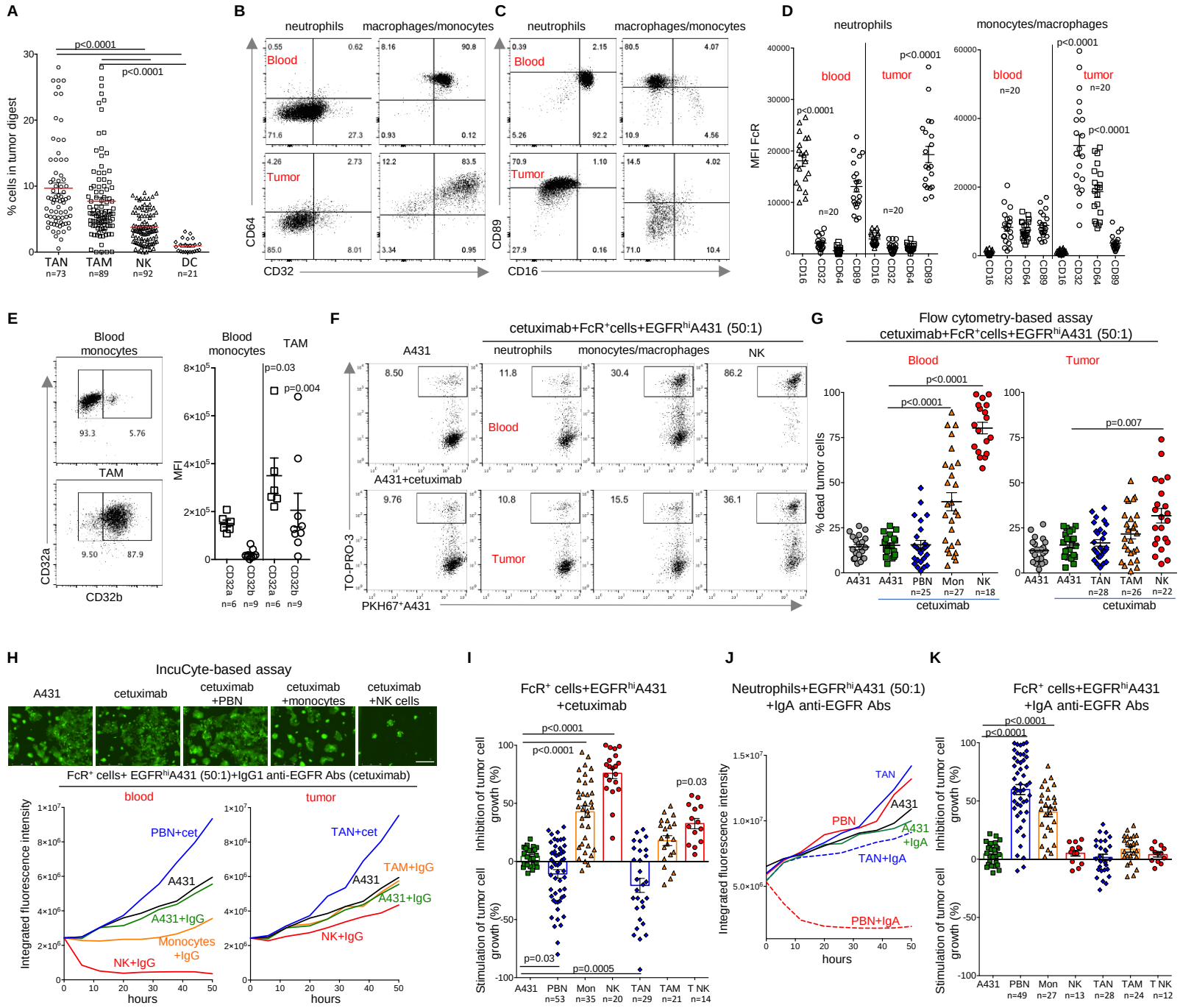

Figure 2

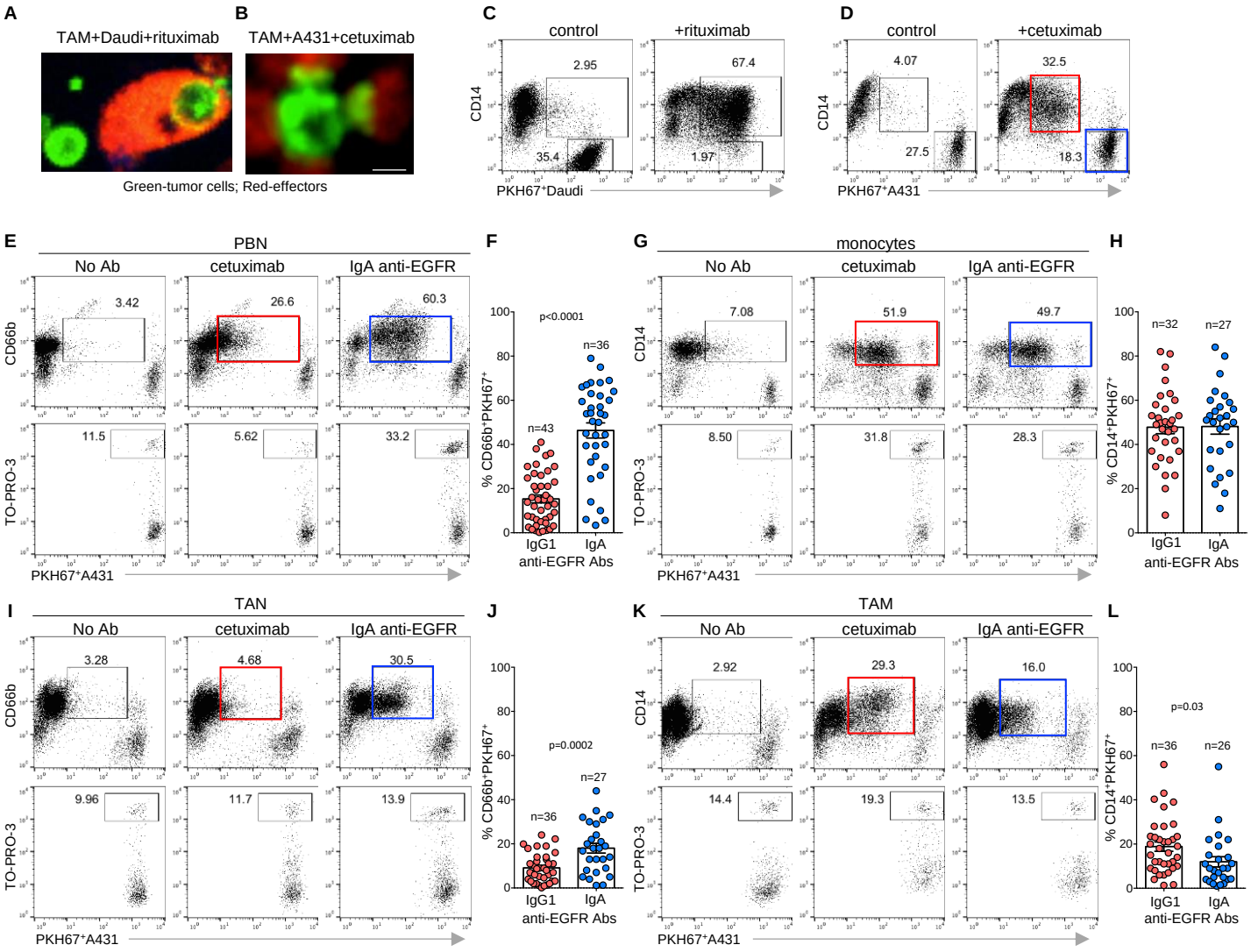

Figure 3

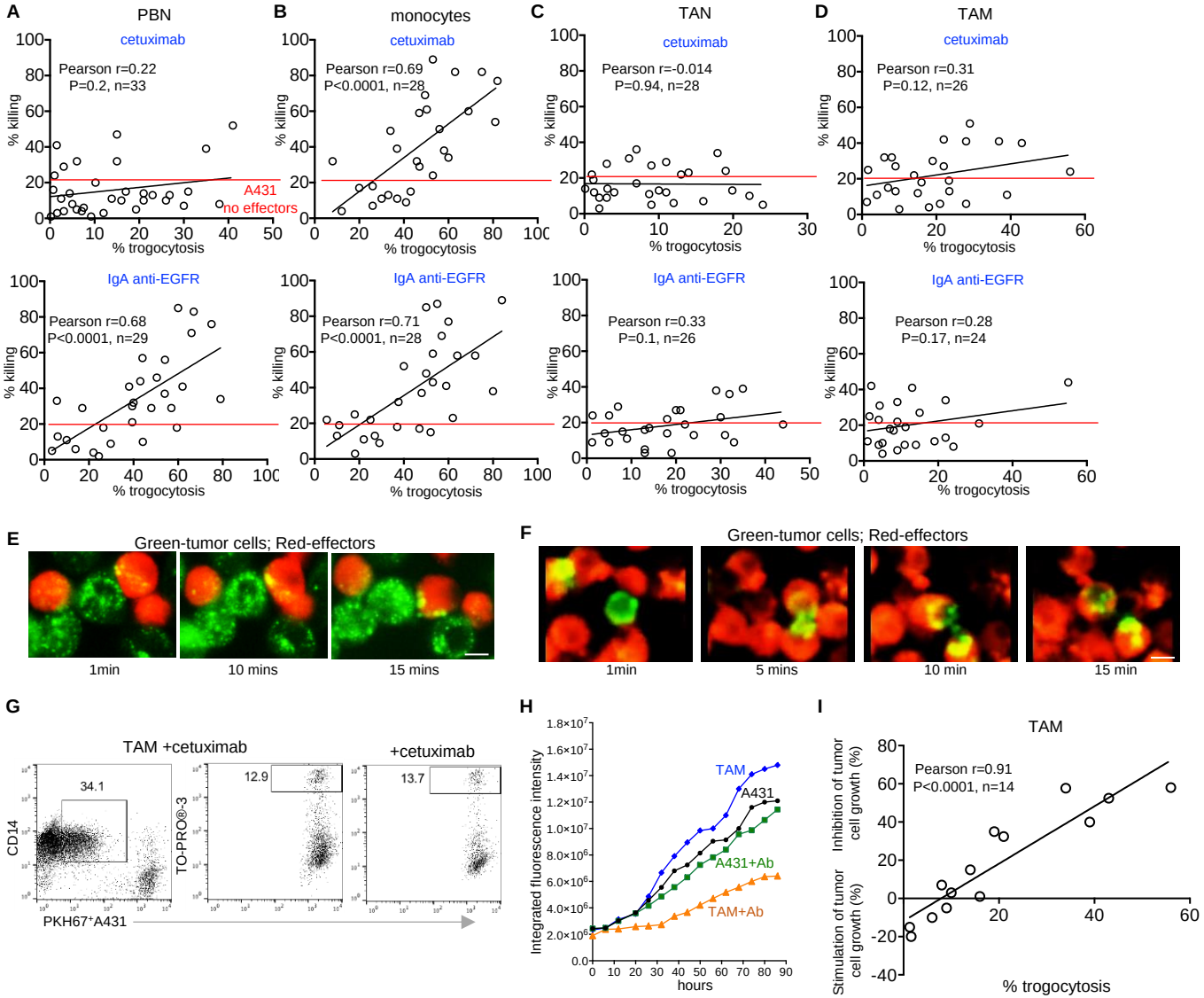

Figure 4

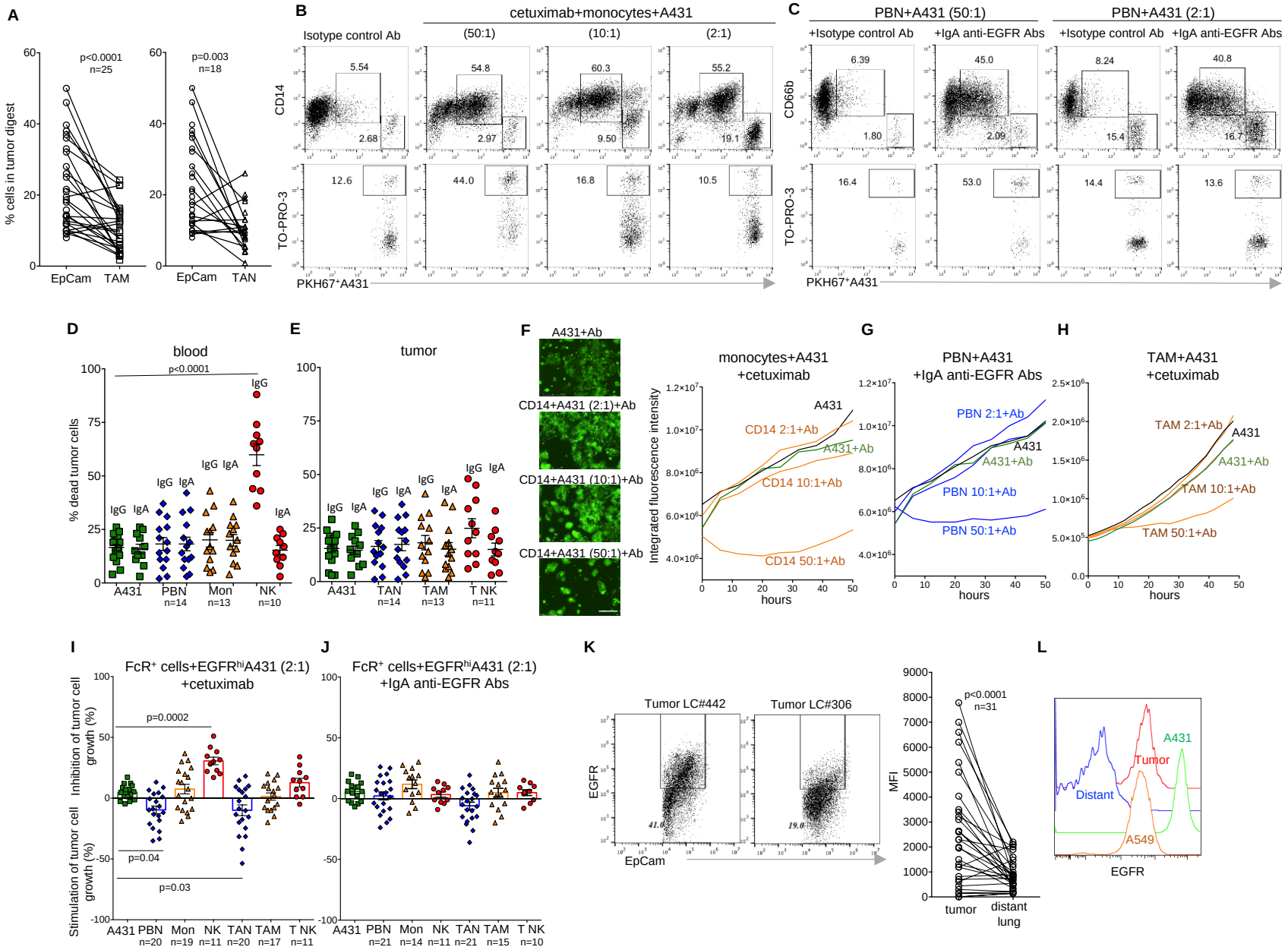

Figure 5

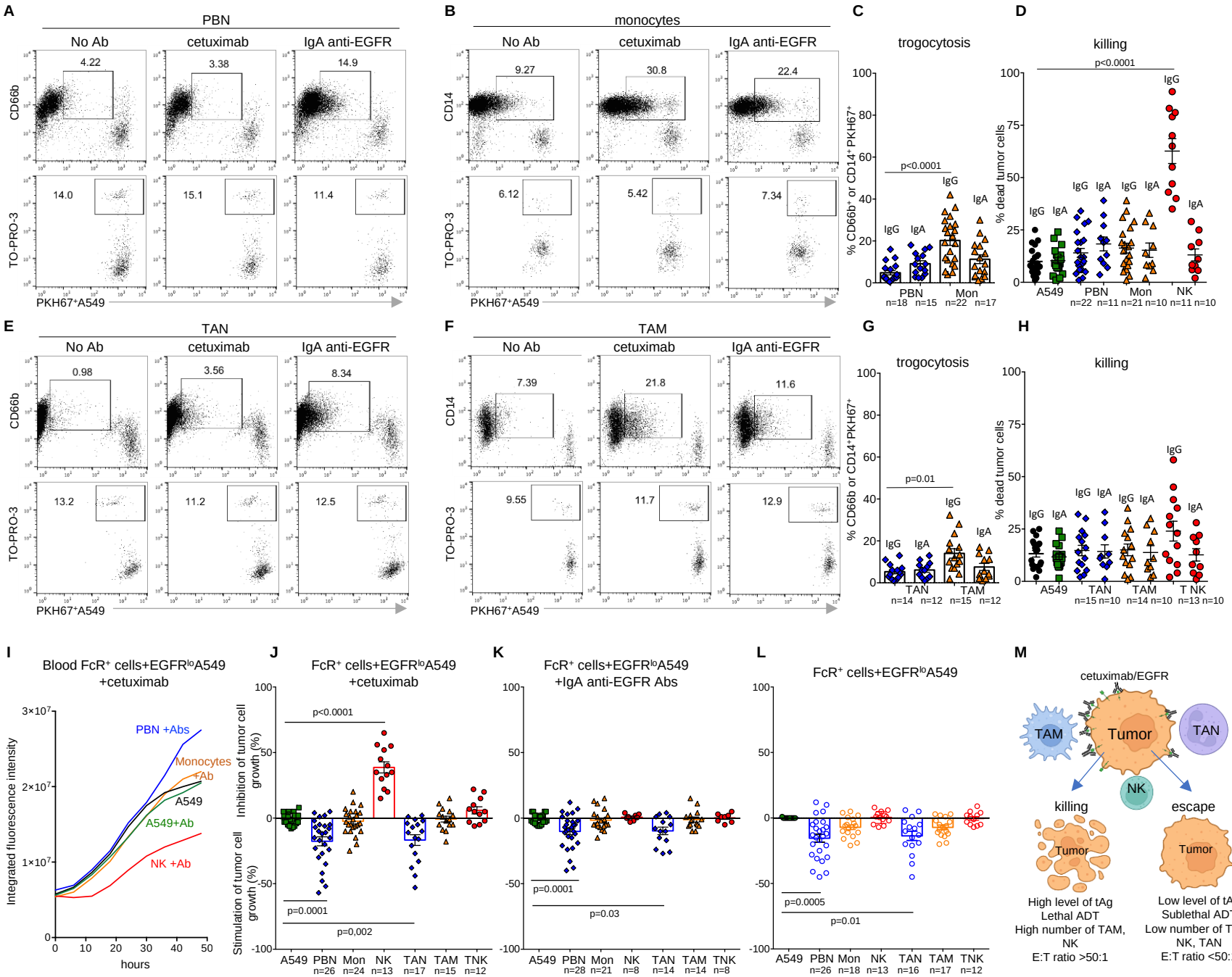

Figure 6

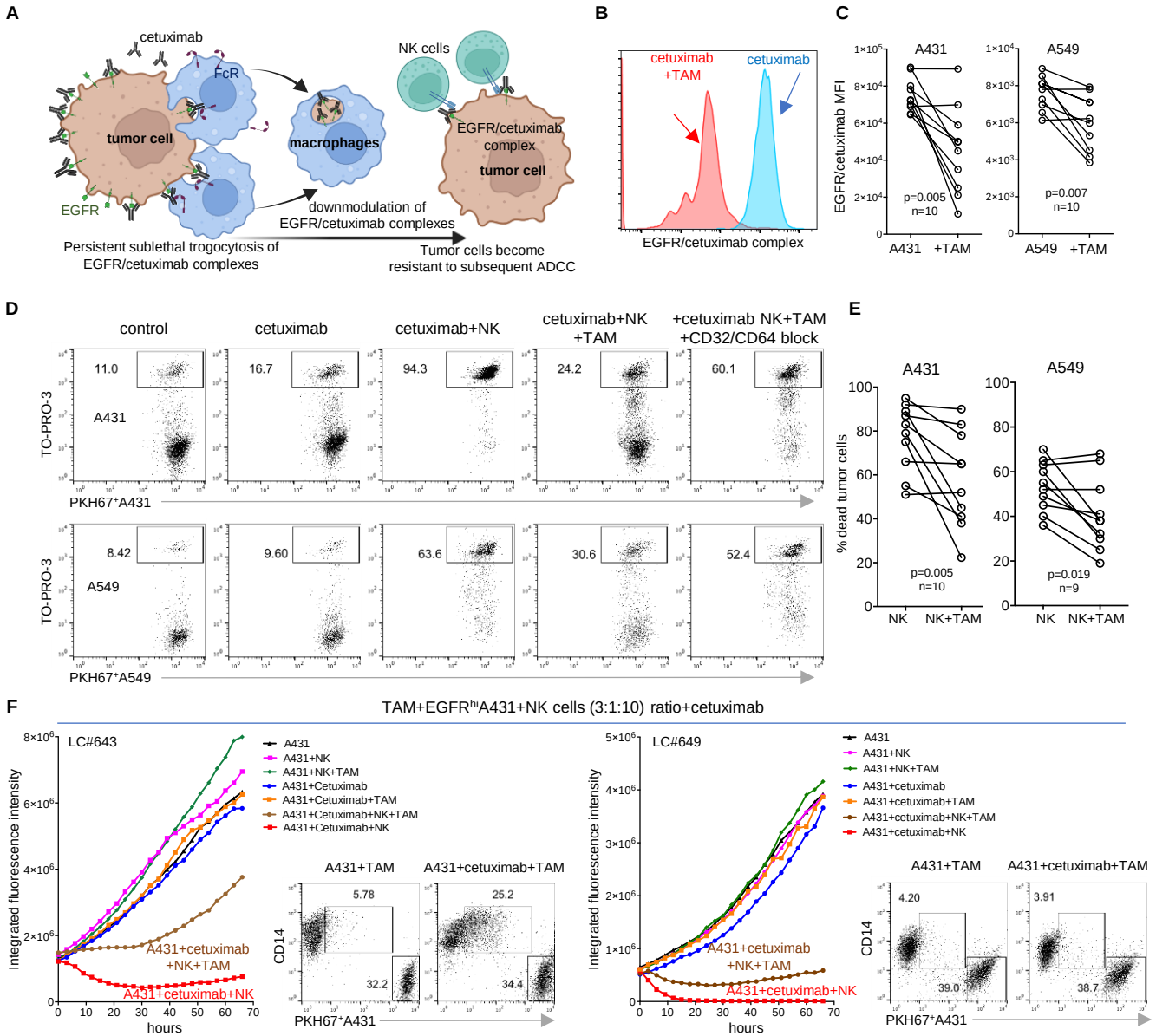

Figure 7